

## CHAPTER 2

# PROPAGATION OF THE PRESSURE PULSE

It is the propagation of the pulse that determines the pressure gradient during the flow at every location in the arterial tree, so it is important to begin the mathematical analysis of arterial fluid mechanics with a description of this propagation. The most concise and easily comprehensible outline of the subject is that by Lighthill (1975, chapter 12), and I shall frequently refer to his account in what follows.

### **2.1 One-dimensional theory, uniform tube, inviscid fluid**

#### *2.1.1 Basic theory*

It is necessary, as in most branches of applied mathematics, to analyse a simple model before introducing the many modifying features present in reality. We therefore start by considering the propagation of pressure waves in a straight, uniform, elastic tube, whose undisturbed cross-sectional area and elastic properties are independent of the longitudinal coordinate,  $x$ . We also take the blood to be inviscid, as well as being homogeneous and incompressible (density  $\rho$ ); the last two assumptions are made throughout this book. The neglect of viscosity is based on the observation (§§ 1.2, 1.3) that the velocity profiles in large arteries are approximately flat, suggesting that the effect of viscosity is confined to thin boundary layers on the walls; this is confirmed mathematically below. We further suppose that the wavelengths of all disturbances of interest are long compared with the tube diameter, so that the velocity profile will remain flat at all times, and the motion of the blood can be represented by the longitudinal velocity component  $u(x, t)$ , where  $t$  is the time. In any comparison with experiment,  $u$  would correspond to the average velocity across the cross-section.

In this one-dimensional model, the (excess) pressure is taken to be  $p(x, t)$  and the tube cross-sectional area to be  $A(x, t)$ .

The equation of mass conservation is

$$A_t + (uA)_x = 0, \quad (2.1)$$

where a suffix denotes partial differentiation, and the momentum equation is

$$u_t + uu_x + (1/\rho)p_x = 0. \quad (2.2)$$

The elastic properties of the tube wall are taken to be represented by a single-valued relation between  $p$  and  $A$ :

$$p = P(A). \quad (2.3)$$

This assumption neglects many features exhibited by a real artery, such as (a) the effect of distension at one value of  $x$  on the value of  $A$  at another, and (b) the viscoelastic nature of the wall. However, it is the simplest assumption consistent with the one-dimensional model, and  $P(A)$  can, in practice, be specified by virtue of the experiments described in § 1.1. Note too that, since  $p$  is the *excess* pressure, the *transmural* pressure of an artery, as well as its undisturbed cross-sectional area and elastic properties, will normally depend on  $x$  because of the hydrostatic pressure gradient inside the vessel but not outside.

The distensibility of the tube, from (1.5), is

$$D = 1/[AP'(A)];$$

we define a velocity  $c$  given by

$$c^2 = (\rho D)^{-1} = (A/\rho)P'(A), \quad (2.4)$$

and the last term in (2.2) becomes  $c^2 A_x/A$ . The familiar Riemannian theory for one-dimensional waves (see, for example, Lighthill, 1978, § 2.8) can now be used: adding  $\pm c/A$  times (2.1) to (2.2) leads to the conclusion that, on the characteristic curves  $C_{\pm}$  such that

$$dx/dt = u \pm c, \quad (2.5)$$

the quantities (Riemann invariants)

$$R_{\pm} = \frac{1}{2} \left[ u \pm \int_{A_0}^A \frac{c}{A} dA \right] \quad (2.6)$$

are constants, where  $A_0$  is the undisturbed area. Thus non-linear waves are propagated in the  $\pm x$ -directions with speeds  $u \pm c$ .

If at all times  $c \gg u$ , the theory can be linearised, (2.1) and (2.2) can be combined into the wave equation

$$p_u = c^2 p_{xx},$$

and any pressure disturbance is predicted to propagate (in either direction) with constant speed  $c_0$ , where the suffix zero means that the quantities in (2.4) are to be evaluated in the undisturbed state. If a mean fluid velocity  $U_0$  were present in the tube, and if  $u \ll U_0$ , the theory could again be linearised, and the speeds of propagation of the wave ( $U_0 \pm c_0$ ) would still be constant.

For the case of a circular tube of wall thickness  $h$  and undisturbed diameter  $d$ , whose response to circumferential stresses can be represented by an effective incremental Young's modulus  $E$ , and provided no additional longitudinal stresses are applied (so that the tube will shorten when it is distended), then  $D$  is given by (1.6) without the factor  $(1 - \sigma^2)$ , and

$$c_0 = (Eh/\rho d)^{1/2}. \quad (2.7a)$$

If the longitudinal tethering of artery walls is taken into account, so that radial stretch induces longitudinal tension,  $D$  is given by (1.6a) or (1.6b) and  $c_0$  by

$$\begin{aligned} c_0 &= (Eh/\rho d)^{1/2} (1 - \sigma_{\theta x} \sigma_{x\theta})^{-1/2} \\ &\approx 1.15 (Eh/\rho d)^{1/2} \end{aligned} \quad (2.7b)$$

when  $\sigma_{x\theta} = \sigma_{\theta x} = 0.5$ .

The linear theory leading to (2.7a) was first performed by Young (1809), and that value of  $c_0$  is known as the Moens–Korteweg wave speed after two Dutch scientists who rediscovered it in 1878.

### 2.1.2 Comparison with experiment

If values of  $E$  measured in static experiments on arteries are inserted into (2.7a), then values of  $c_0$  are predicted that range from about  $5.8 \text{ m s}^{-1}$  in the aorta (of a dog) to nearly  $10 \text{ m s}^{-1}$  in peripheral arteries (see table 1.1). These predictions can be compared with measured values of the wave speed, which are also quoted in table 1.1 (see Bergel (1972b) or McDonald (1974, p. 418) for more extensive lists and references to the original experiments). Wave speed is not in fact very easy to measure *in vivo* because of the

change in shape of the pressure pulse with distance along the arterial tree (fig. 1.14 or 1.17), which is primarily a consequence of wave reflection (§ 2.3). The only reliable methods are *either* to measure the speed of propagation of the initial part (the 'foot') of the pulse where the pressure begins to rise (McDonald, 1974, p. 394), *or* to introduce short trains of artificial, high-frequency, sinusoidal waves and measure their propagation speed (Anliker, Hinstead & Ogden, 1968*a*). These methods allow a pair of pressure measurements to be made (with two manometers) before reflected waves have time to distort the signal. The two methods give similar results, although the frequencies used by Anliker *et al.* (1968*a*) are higher than those important in the pressure pulse. Note that the increase of wave speed with distance from the heart means that any measured values can be regarded only as averages over the distance between manometers.

Considering the crudeness of the linear theory leading to (2.7*a*), the agreement between prediction and observation (table 1.1) appears to be remarkably good. Actually the agreement is not quite as good as indicated, because (*a*) the dynamic, not the static, Young's modulus should be used, which is greater by a factor of about 1.2 (p. 20), and (*b*) (2.7*b*) should be used instead of (2.7*a*). This has the effect of increasing the predictions of  $c_0$  by about 25%, so that they exceed the observations considerably, and we should seek mechanisms that might reduce the predicted wave speed. Nevertheless, the qualitative agreement suggests that the simple linear model, incorporating merely wall elasticity and fluid inertia, contains the most essential features of pulse propagation.

The linear theory indicates that the speed of propagation of small-amplitude waves,  $c_0$ , depends on the distensibility of the tube in its undisturbed state. But as we saw in § 1.1, the distensibility of arteries falls as the distending pressure, and hence the undisturbed cross-sectional area, increases. Therefore the wave speed should increase with blood pressure. In particular, the wave speed during systole ( $p \approx 16 \text{ kN m}^{-2}$ ) will be greater than that during diastole ( $p \approx 10.7 \text{ kN m}^{-2}$ ); if the difference between systolic and diastolic wave speed is significant, then the use of linear theory to describe the propagation of the pulse would be inappropriate. This was tested experimentally in the canine aorta by Hinstead & Anliker

(1973), who superimposed short trains of high-frequency waves on the natural pressure pulse during both systole and diastole, and measured the propagation speed. Their results were complicated by the fact (already noted) that the propagation speed is increased by the local average convection velocity, which is zero in diastole but significant in systole. They therefore measured the speed of propagation upstream as well as downstream, and took the average to indicate the intrinsic wave speed at the pressure concerned. The difference between upstream and downstream wave speeds normally reached about  $1 \text{ m s}^{-1}$  in systole (indicating a rather low peak flow velocity of  $0.5 \text{ m s}^{-1}$ ), but in some animals rose to  $2 \text{ m s}^{-1}$ . More important, perhaps, is the fact that the intrinsic wave speed was greater in systole than in diastole by about  $1 \text{ m s}^{-1}$ , or 20% of its normal measured value (the 'foot-to-foot' wave speed should be roughly the same as the diastolic value, since the pressure and flow velocity are only beginning to increase when this part of the pulse passes). These results were confirmed and extended by experiments in which the aorta was occluded below or above the measuring site, so that the mean pressure could be raised or lowered beyond the normal range (fig. 2.1).

As well as the non-linearity of the pressure-area relation, fluid mechanical non-linearities may also affect the validity of linear theory if  $u/c$  is not much less than 1 at all times. In the thoracic aorta of a normal dog,  $u_{\text{max}}/c \approx 0.20\text{--}0.25$  (see table 1.1), and a similar ratio obtains in man. The ratio becomes smaller in smaller arteries, where  $u_{\text{max}}$  decreases and  $c$  increases. Thus the crude linear theory is expected to give a reasonable first approximation to the description of wave propagation, with errors of at most about 25% arising from fluid mechanical and elastic non-linearities in the aorta. The fluid mechanical non-linearities become less important in smaller arteries, but the elastic ones do not because the amplitude of the pressure pulse increases peripherally (fig. 1.14).

Non-linearities assume greater importance in abnormal conditions where either (a) the artery walls become very distensible, so that both  $c$  falls (increasing  $u_{\text{max}}/c$ ) and the area change for a given pressure pulse increases, or (b) the output of the ventricle per beat is significantly increased, so that  $u_{\text{max}}$  is increased. The latter occurs, for example, when the aortic valve does not close properly (i.e. is

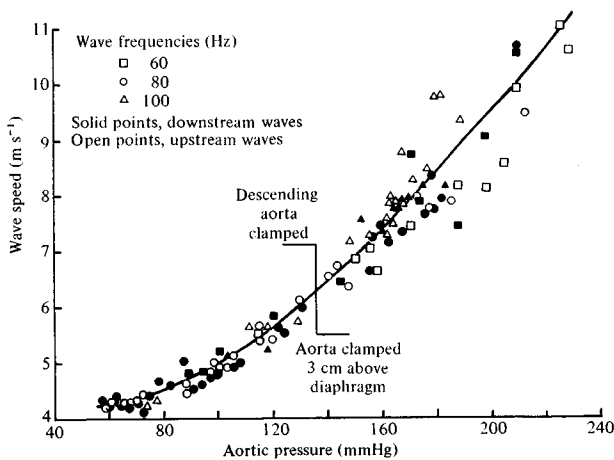


Fig. 2.1. Wave speed plotted against pressure in the canine aorta. Different pressures were obtained by occluding the aorta either above or below the test segment. Each point represents the average of a peak and a successive trough of a small sine wave. (After Hstand & Anliker, 1973.)

'incompetent'), so that a large proportion of the blood ejected by the ventricle in systole flows back into it again in diastole. The heart responds to this condition (over a long period) by becoming greatly enlarged and increasing the volume ejected in an attempt to maintain the peripheral circulation. The amplitude of the pulse is then very large; indeed, one way of diagnosing the condition is by a very strong pulse in the limbs, called the arterial 'pistol shot'. It is virtually certain that non-linear theory is required to describe such a pulse; indeed, Anliker, Rockwell & Ogden (1971) propose that it is the manifestation of a hydraulic jump, or shock, in the arterial system (see below).

### 2.1.3 Attenuation

Before developing a non-linear analysis, we should consider one further aspect of the experiments of Anliker *et al.* (1968*a*) and of Hstand & Anliker (1973). This concerns the attenuation of waves, which must take place in any real system, but which the peaking of the pressure pulse (fig. 1.14(*a*)) effectively obscures in large arteries. The introduction of short trains of high-frequency waves is an ideal way of studying attenuation, and Anliker *et al.* (1968*a*)

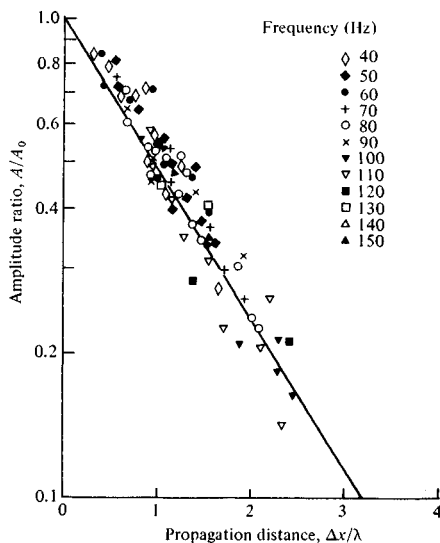


Fig. 2.2. Attenuation of sinusoidal pressure waves in a dog's aorta, with  $A/A_0$  plotted on a logarithmic scale against propagation distance in wavelengths.  $\Delta x = 6$  cm; attenuation constant  $k = 0.75$ . (After Anliker, 1972.)

were able to show convincingly that small-amplitude sinusoidal pressure waves in the aorta had a constant rate of attenuation per wavelength (fig. 2.2). That is, the pressure in the artery takes the form

$$p = p_1 + p_2 e^{-kx/\lambda} e^{i\omega(t-x/c)}, \quad (2.8)$$

where  $p_1$  is the underlying blood pressure,  $p_2$  is a measure of the amplitude at  $x = 0$ , and  $\lambda = 2\pi c/\omega$  is the wavelength of the wave. Anliker *et al.* (1968a) found that the attenuation constant  $k$  normally lies between 0.7 and 1.0 for waves propagating peripherally in the canine aorta (i.e. attenuation of 50–63% per wavelength; this would have a small effect on the natural pulse in the aorta because the wavelength for a fundamental frequency of 2 Hz is at least 2.5 m). Hstrand & Anliker (1973) found that upstream propagated waves suffer greater attenuation, with  $k$  between 1.3 and 1.5.

The source of this wave attenuation lies primarily in the visco-elastic properties of the vessel wall. This follows from calculations

made on the assumption that all attenuation comes from blood viscosity, which predict  $k \approx 0.04$  for the aorta (§ 2.2). However, if we use a complex Young's modulus (or distensibility) to describe the viscoelastic properties of the artery wall, i.e.  $E_\theta = E_{\text{dyn}} + i\eta\omega$  (p. 20), and put this into (2.7*a* or *b*) for  $c$ , we deduce a value of  $k$  given by

$$k = 2\pi \tan \frac{1}{2}\theta \quad \text{where} \quad \tan \theta = \eta\omega/E_{\text{dyn}}. \quad (2.9)$$

This gives a value of  $k$  between 0.47 and 0.62 for  $\eta\omega/E_{\text{dyn}}$  between 0.15 and 0.2, and, combined with the prediction for blood viscosity, approximately accounts for the observed  $k$  of 0.7–1.0.† It is not obvious why the attenuation of upstream waves in arteries should be significantly greater; it may be related to the taper of the arteries (§ 2.3).

We may note further that Anliker, Wells & Ogden (1969) measured the propagation characteristics of pressure waves travelling towards the heart in the canine vena cava by a method similar to that used in arteries. They found a wave speed rising from about  $2.5 \text{ m s}^{-1}$  at a (physiological) distending pressure of  $1 \text{ kN m}^{-2}$  to  $5.0 \text{ m s}^{-1}$  at a distending pressure of  $2.3 \text{ kN m}^{-2}$ . They also found approximately constant attenuation per wavelength, but with a value of  $k$  that ranged from 0.6 to 3.3 in different animals at different pressures.

#### 2.1.4 *Non-linear effects*

The theory leading to (2.5) and (2.6) already incorporates non-linearities; their effect in such an inviscid, uniform-tube model is to cause the front of any wave to steepen, because the wave speed increases with both  $u$  and  $p$ . Such steepening of the pressure pulse is commonly observed (§ 1.2). Ultimately this steepening creates a discontinuity, and a shock is formed. Of course, the non-dissipative equations (2.1)–(2.3), from which the existence of a shock is predicted, will break down before a discontinuity actually appears, because the neglected dissipative terms become important. When a steady shock (or wavefront) is set up, these terms exactly balance the non-linear terms that are responsible for the steepening. The

† Some very recent experiments suggest that there is still a considerable gap, however (Dr C. D. Bertram, personal communication).



following prediction of when the shock will form will be accurate only if the dissipative terms are very small except for a short time before the steady state is set up. Suppose that blood is ejected from the ventricle ( $x = 0$ ) into a uniform tube with velocity  $U(t)$ , which is positive for  $t \geq 0$  (at least for some time) and zero for  $t < 0$ . Assume the flow and the tube to be undisturbed for  $t < 0$ . Then the usual methods (Lighthill, 1978) can be applied to the  $x > 0$ ,  $t > 0$  quadrant of the  $(x, t)$ -plane. Write

$$\int_{A_0}^A \frac{c}{A} dA = V(c)$$

where  $V(c_0) = 0$  and  $V(c)$  is assumed to be a single-valued function with a unique inverse. For  $x > c_0 t$ ,  $u = 0$  and  $c = c_0$ . Now all  $C_-$  characteristics originate (at  $t = 0$ ) in the region  $x > c_0 t$ , so that, from (2.6),  $u = V(c)$  everywhere. Hence, on the  $C_+$  characteristics in the region  $0 < x < c_0 t$ ,  $u + V(c) = 2u = \text{constant}$ , and so  $c (= c(u))$  is also constant, and the characteristics are straight, a typical one having the equation

$$x = \{U(\tau) + c[U(\tau)]\}(t - \tau).$$

Two  $C_+$  characteristics first cross, and hence a shock is formed, at a value of  $t$  equal to the minimum of

$$\tau + F[U(\tau)] / \dot{U}(\tau) F'[U(\tau)] \quad (2.10)$$

for values of  $\tau$  such that  $\dot{U}(\tau) > 0$ , where  $F(U) \equiv U + c(U)$ .

A simple example of a function  $P(A)$ , which has the property that the tube becomes less distensible as  $A$  increases, is

$$P = \frac{1}{2} \rho c_0^2 A^2 / A_0^2 + \text{constant}. \quad (2.11)$$

This is very convenient for working out numerical examples since  $c = c_0 A / A_0$  and  $V(c) = c - c_0$ , so that  $F(U) = 2U + c_0$ . Let us also choose a simple but realistic form for  $U(t)$ :

$$\left. \begin{aligned} U(t) &= U_0 [1 - (1 - t/t_0)^2] & 0 \leq t \leq 2t_0, \\ &= 0 & t > 2t_0; \end{aligned} \right\} \quad (2.12)$$

this is plotted in fig. 2.3;  $2t_0$  is the duration of systole, while  $U_0$  is the maximum systolic velocity. The minimum value of (2.10) for  $0 \leq \tau \leq t_0$  (values of  $\tau$  for which  $\dot{U} > 0$ ) occurs at  $\tau = 0$ , because  $U$  is an increasing function and  $\dot{U}$  a decreasing function. The time at which

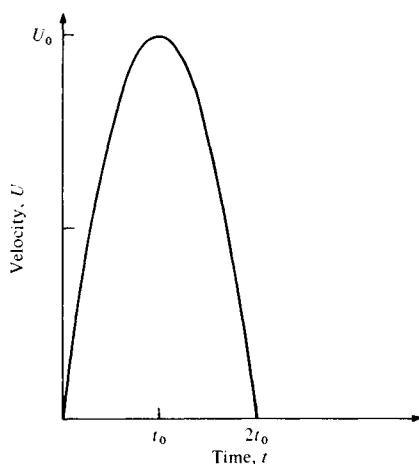


Fig. 2.3. Sketch of the velocity waveform used in the calculation of the time and place at which a hydraulic jump is expected to develop.

a shock forms is therefore  $t_s = c_0 t_0 / 4 U_0$ , and the position at which it forms is  $x_s = c_0^2 t_0 / 4 U_0$ . For a normal dog's aorta, with  $c_0 \approx 5 \text{ m s}^{-1}$ ,  $U_0 \approx 1.2 \text{ m s}^{-1}$ ,  $t_0 \approx \frac{1}{12} \text{ s}$  (based on a heart-rate of 2 Hz, and systole lasting one-third of the cycle),  $t_s$  is about 0.09 s, and  $x_s$  about 43 cm. This is somewhat greater than the length of the aorta, and would in practice be greater still because of the increase of  $c_0$  and decrease of  $U_0$  with distance from the heart; dissipative effects would also increase the prediction. Thus the occurrence of shocks is not normally to be expected. However, if  $U_0$  is increased to, say,  $3 \text{ m s}^{-1}$  in a diseased system,  $x_s$  is predicted to be only about 17 cm, which is quite feasible, and means that there is a *prima facie* case for examining the mechanics of shocks in elastic tubes.

We analyse such a shock, represented as a step jump in  $A$ ,  $u$  and  $p$  in the same way as a hydraulic jump on a channel (Lighthill, 1978, § 2.12). Take axes fixed in the shock in order to make the problem steady, and consider the flux of mass, momentum and energy across the boundaries of the control surface  $S$  (fig. 2.4). Conservation of mass implies

$$u_1 A_1 = u_2 A_2, \quad (2.13)$$

where subscripts 1,2 represent upstream and downstream conditions respectively; note that  $u_1$  is actually the speed of propagation

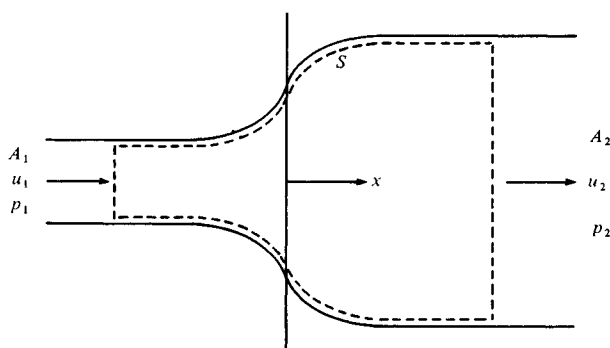


Fig. 2.4. Control surface,  $S$ , used to derive the jump conditions for a hydraulic jump in an elastic tube; the axes are fixed in the shock.

of the shock into fluid initially at rest. We take  $A_1 < A_2$  as drawn. Conservation of momentum is a bit more complicated than in the case of the hydraulic jump, because of the contribution to the momentum flux of the pressure exerted on the fluid by the non-parallel walls of the shock. The equation is

$$A_1(p_1 + \rho u_1^2) + \int_1^2 p \, dA = A_2(p_2 + \rho u_2^2), \quad (2.14)$$

where the integral is the extra pressure force term. We must recognise that within the shock our simple model of the elasticity might break down, so that  $p$  in the integral may not be equal to  $P(A)$  (see (2.3)). Finally, energy conservation requires that energy cannot be gained by fluid as it passes the shock, i.e.

$$p_1 + \frac{1}{2}\rho u_1^2 = p_2 + \frac{1}{2}\rho u_2^2 + R, \quad (2.15)$$

where  $R \geq 0$ .

These equations can be manipulated in various ways. Equations (2.13) and (2.14) lead to

$$\rho u_1^2 (A_1/A_2)(A_2 - A_1) = \bar{A}(p_2 - p_1), \quad (2.16)$$

where we define

$$\begin{aligned} \bar{A}(p_2 - p_1) &= A_2 p_2 - A_1 p_1 - \int_1^2 p \, dA \\ &= \int_1^2 A \, dP - \int_1^2 (p - P) \, dA. \end{aligned}$$

The first term on the right is equal to  $\int_1^2 \rho c^2 dA$ , which is greater than  $\rho c_1^2(A_2 - A_1)$  as long as  $c^2$  is a monotonically increasing function of  $A$  and  $A_2 > A_1$  (as we suppose). Thus if  $p = P(A)$  throughout the shock, then

$$(u_1^2/c_1^2) > (A_2/A_1) > 1.$$

Similarly we can show  $u_2^2 < c_2^2$  in this case. Thus upstream of the shock the flow is supercritical, and downstream it is subcritical, as for hydraulic jumps. However, this result may not be true if  $p \neq P(A)$  in the shock and if  $\int_1^2 (p - P) dA$  is sufficiently large.

Equations (2.13)–(2.15) also yield

$$R\bar{A}/\rho(u_1^2 - u_2^2) = \frac{1}{2}\bar{A} - A_1A_2/(A_1 + A_2). \quad (2.17)$$

Again, if  $p = P(A)$  in the shock,  $R > 0$  requires  $u_1 > u_2$  (as shown in fig. 2.4) as long as

$$\frac{\int_1^2 A(dP/dA) dA}{P(A_2) - P(A_1)} > \frac{2A_1A_2}{A_1 + A_2}. \quad (2.18)$$

This condition imposes a constraint on the function  $P(A)$ , that the average area, weighted by the slope of the pressure–area curve, should be greater than the harmonic mean area. The condition (2.18) is satisfied when  $P(A)$  is a linear function,

$$P = \alpha + \beta A \quad (\beta > 0),$$

for the left-hand side is then equal to  $\frac{1}{2}(A_1 + A_2)$ ; clearly, therefore, (2.18) is satisfied for any function  $P(A)$  for which  $dP/dA$  increases with  $A$ , including our simple quadratic case (2.11). It is interesting to note that the two sides of (2.18) are equal for the case

$$P = \frac{1}{2}\rho c_0^2(1 - A_0^2/A^2),$$

chosen by Olsen & Shapiro (1967) to represent a rubber tube. Thus a discontinuity can propagate without any energy loss, which explains Olsen & Shapiro's observation that arbitrary non-linear waves could propagate without change of form.

We have concluded, then, that for realistic pressure–area relations, obtaining throughout the shock, there should be some energy loss in the fluid ( $R > 0$ ). This energy loss, as in the case of the hydraulic jump, may be associated with the significant viscous dissipation that would occur if the flow emerging from the shock

formed a separated jet that became turbulent, or (in the case of a weak shock) it could be propagated away in non-linear waves, for which a two-dimensional theory would have to be developed. However, there is another source of dissipation available in the case of blood vessels, and that is the viscoelastic properties of their walls. We have seen already that this is responsible for much more wave attenuation than blood viscosity, and the analysis below indicates that it is the most probable source of dissipation for cardiovascular shocks, since the presence of viscoelasticity would limit the wall slope at the shock, even for a strong shock, to a value below that at which the blood flow would separate. Thus significant turbulent dissipation is unlikely to occur.

If all energy loss takes place in the vessel walls, there is none in the fluid, and  $R$  in (2.15) is zero. However  $p \neq P(A)$  throughout the shock because energy is dissipated at any location as the vessel area increases. This means that, with axes fixed in the tube wall, we should write

$$p = P(A) + N(A, \partial A / \partial t), \quad (2.19)$$

where  $N$  is a monotonically increasing function of  $\partial A / \partial t$  with  $N(A, 0) = 0$  (Kivity & Collins, 1974). The simplest form of  $N$ , corresponding to the complex Young's modulus used above, is

$$N = g(A)(\partial A / \partial t). \quad (2.20)$$

For a small-amplitude sinusoidal wave of the form  $e^{i\omega(t-x/c)}$ , superimposed on a basic state of cross-sectional area  $A_0$ , the linearised theory based on (2.1) and (2.2) leads to the prediction that

$$D^{-1} = \rho c^2 = A_0 [P'(A_0) + i\omega g(A_0)].$$

Thus we have

$$\eta\omega / E_{\text{dyn}} = \text{Im}(D^{-1}) / \text{Re}(D^{-1}) = \omega g(A_0) / P'(A_0), \quad (2.21)$$

which is related to the attenuation constant  $k$ , (2.9). Note that since  $\eta\omega$  is observed to be independent of  $\omega$ ,  $g(A_0)$  will be frequency-dependent.

If we now revert to the frame of reference fixed in the shock (fig. 2.4), the problem once more becomes steady,  $\partial/\partial t$  becomes

$u_1 \partial/\partial x$  and we obtain

$$p = P(A) + u_1 g(A) \, dA/dx.$$

Thus

$$\int_1^2 (p - P) \, dA = u_1 \int_1^2 g(A) \left( \frac{dA}{dx} \right)^2 dx > 0,$$

and (2.17) with  $R = 0$  leads to

$$u_1 \int_1^2 g(A) \left( \frac{dA}{dx} \right)^2 dx = \int_1^2 A \frac{dP}{dA} \, dA - \frac{2A_1 A_2}{A_1 + A_2} [P(A_2) - P(A_1)]. \quad (2.22)$$

For a shock corresponding to a given area change, (2.22) will yield an estimate for the slope (related to  $dA/dx$ ) as long as  $u_1$  is known; (2.13), combined with (2.15) with  $R = 0$ , yields

$$\rho u_1^2 = [2A_2^2/(A_2^2 - A_1^2)][P(A_2) - P(A_1)], \quad (2.23)$$

which determines  $u_1$ .

We consider a particular example in which  $P(A)$  is a quadratic function, given by (2.11), and  $g(A)$  is a constant,  $\rho g_0$ , so that (2.23) gives

$$u_1 = A_2 c_0 / A_0$$

and (2.22) gives

$$g_0 \int_1^2 \left( \frac{dA}{dx} \right)^2 dx = \frac{c_0(A_2 - A_1)^3}{3A_0 A_2}.$$

To estimate the wall slope, let  $L$  be a scale for the distance over which the area change  $\Delta A = A_2 - A_1$  takes place; then

$$\Delta A/L = c_0(\Delta A)^2/3g_0 A_0 A_2. \quad (2.24)$$

For the aorta, suppose  $A_1 = A_0 \approx 1.8 \text{ cm}^2$ , and take  $\Delta A = 0.7 \text{ cm}^2$  normally (corresponding to a pressure pulse of  $5.3 \text{ kN m}^{-2}$ ) and take  $\Delta A = 1.8 \text{ cm}^2$  in a diseased state (when the pressure pulse is  $13.3 \text{ kN m}^{-2}$ ); then  $(\Delta A)^2/3A_0 A_2$  varies between 0.04 and 0.17. We take  $c_0 = 5 \text{ m s}^{-1}$  and from (2.21) with  $\eta\omega/E_{\text{dyn}} = \frac{1}{6}$  and  $\omega = 20\pi$  (taken to be a typical frequency of shock passage) we take  $g_0 = 3.7 \times 10^3 \text{ s}^{-1}$ , and therefore obtain

$$\Delta A/L \approx 0.005 \text{ cm } (\Delta A = 0.7 \text{ cm}^2) \quad \text{or} \quad 0.023 \text{ cm } (\Delta A = 1.8 \text{ cm}^2).$$

If the tube is circular, this corresponds to a wall slope of  $0.05^\circ$  ( $\Delta A = 0.7 \text{ cm}^2$ ) or  $0.22^\circ$  ( $\Delta A = 1.8 \text{ cm}^2$ ), which in either case is too gradual for flow separation to take place. The slope would be greater only if  $\omega$  were greater and  $g_0$  smaller.

In this particularly simple example, the 'shock structure' can be calculated exactly, as shown by Kivity & Collins (1974). The constancy of the flow-rate,  $uA$ , and pressure head,  $p + \frac{1}{2}\rho u^2$ , means that (2.19) can be written

$$N(A, u_1 dA/dx) = P(A_1) - P(A_2) + \frac{1}{2}\rho u_1^2(1 - A_1^2/A^2).$$

Taking  $P(A)$  of the form (2.11), and  $N$  of the form (2.20) with  $g(A) = \rho g_0$ , and recognising that  $A_1 = A_0$  and  $u_1 = A_2 c_0/A_0$ , we obtain

$$(2g_0 A_2/c_0) d\alpha/dx = (1/\alpha^2)(\alpha_2^2 - \alpha^2)(\alpha^2 - 1),$$

where  $\alpha = A/A_0$  and  $\alpha_2 = A_2/A_0$ . This can be integrated to give

$$\left(\frac{\alpha-1}{\alpha+1}\right)\left(\frac{\alpha_2+\alpha}{\alpha_2-\alpha}\right)\alpha^3 = \exp\left[\frac{c_0}{g_0 A_0} \frac{(\alpha_2^2-1)}{\alpha_2}(x-x_0)\right],$$

where  $x_0$  is the location of the shock centre. The longitudinal length-scale revealed by the solution is  $(g_0 A_0/c_0)[\alpha_2/(\alpha_2^2-1)]$ , which agrees dimensionally with (2.24).

The application of this model to arteries is rather unsatisfactory because of the assumption of constant  $g_0$ , since experiments show that  $g_0$  is inversely proportional to  $\omega$  for sinusoidal disturbances of angular frequency  $\omega$  greater than  $4\pi \text{ s}^{-1}$ . Now a suitable choice for  $\omega$  in the case of a passing shock is some multiple,  $\beta$ , of  $2\pi c_0/L$ , where  $L$  is the axial length-scale. But then the quantity  $L$  drops out of (2.24), which serves merely to determine  $\beta$ , and appears to permit an arbitrary value of  $L$ . What this means is that the details of shock thickness and structure in an artery will depend on rather more subtle features of the wall viscoelastic properties than can be described by (2.20) with constant  $g(A)$ . Presumably the low-frequency contributions, describing the slow departure of the tube from its cylindrical shape far upstream and downstream dominate the expression for shock thickness, since a constant  $g_0$  is appropriate there. The problem clearly merits further study. Collins *et al.* (1976) have applied the analysis of Kivity & Collins (1974) to experimentally produced shocks in Silastic tubes, and used their observations

to infer the viscoelastic properties of the tubes. They propose using the same technique in arteries, but the doubts expressed above indicate that their results will have to be examined with caution.

## 2.2 Two-dimensional theory, uniform tube, viscous fluid

While the above one-dimensional approach is believed to contain most of the features pertinent to the pulse wave in arteries modelled as uniform tubes, certain elastic phenomena cannot be described by that theory. Furthermore, the effects of viscosity can be incorporated in a one-dimensional theory only after an analysis of the velocity profile in a parallel-sided tube has been separately performed (Lighthill, 1975, chapter 12). We therefore present here a *linearised* analysis of the axisymmetric motion of a viscous fluid contained in a circular tube whose wall is a viscoelastic, orthotropic membrane, tethered to a rigid external structure by linear constraints. The analysis closely follows and extends the paper of Atabek (1968), which is an excellent example of this type of theory, based on, but going further than, the original work of Womersley (1957). Other relatively recent examples are the papers of Anliker & Dorfman (1970) and of Jones, Anliker & Chang (1971). Most of these papers have examined the effects of the various parameters at great length, but with a purely numerical approach. The purpose of this section is to bring out the main qualitative features of the results in a simple analytical way.

### *Equations of motion of the wall*

Let the undisturbed state of the tube be that of a uniform, circular thin-walled cylinder, radius  $a$ , density  $\rho_w$  and wall thickness  $h$ , with a uniform longitudinal tension  $S$  per unit circumference, and a circumferential tension  $T$  per unit length corresponding to transmural pressure  $P_0$  ( $T = P_0 a$ ). We shall use cylindrical polar coordinates  $(x, r, \theta)$  and restrict attention to axisymmetric disturbances in which no displacements occur in the  $\theta$ -direction (this last condition rules out axisymmetric torsional waves, which have been analysed by Anliker & Maxwell (1966)). Let the displacement of a point in the wall be  $(\xi, \eta, 0)$ , functions of only  $x$  and  $t$ , and let the wall be subjected to *external* stresses  $(X, P_0 + Y, 0)$ . Let the



perturbation tensions in the axial and circumferential directions be  $s'$  and  $t'$  respectively.

The equations of motion of the wall can be deduced from the linearised version of the standard equations of motion of axisymmetric shells (Flügge, 1973), and are

$$\left. \begin{aligned} \rho_w h \frac{\partial^2 \xi}{\partial t^2} &= \frac{(S-T)}{a} \frac{\partial \eta}{\partial x} + \frac{\partial s'}{\partial x} + X, \\ \rho_w h \frac{\partial^2 \eta}{\partial t^2} &= \frac{T\eta}{a^2} - \frac{t'}{a} + T \frac{\partial^2 \eta}{\partial x^2} + Y. \end{aligned} \right\} \quad (2.25)$$

### *Stress-strain relations*

In an orthotropic viscoelastic shell the stress perturbations can be most easily related to the displacements if we restrict attention to sinusoidal disturbances of angular frequency  $\omega$ , in which all variables are proportional to  $e^{i\omega t}$ . Then a linear relation between stress, strain and rate of strain reduces to a linear relation between stress and strain, as long as all variables are allowed to be complex. We obtain

$$\left. \begin{aligned} t' &= B_{11}\eta/a + B_{12} \partial \xi / \partial x, \\ s' &= B_{21}\eta/a + B_{22} \partial \xi / \partial x, \end{aligned} \right\} \quad (2.26)$$

where in terms of (complex) Young's moduli and Poisson's ratios, different in the  $x$ - and  $\theta$ -directions, we have

$$\left. \begin{aligned} B_{11} &= E_\theta h / (1 - \sigma_\theta \sigma_x), \quad B_{22} = E_x h / (1 - \sigma_\theta \sigma_x), \\ B_{12} &= E_\theta h \sigma_x / (1 - \sigma_\theta \sigma_x) = B_{21} = E_x h \sigma_\theta / (1 - \sigma_\theta \sigma_x), \end{aligned} \right\} \quad (2.27)$$

(see Atabek (1968), and Patel & Vaishnav (1972)).

### *Stresses exerted on the wall*

Two types of stress are exerted on the wall. (i) There are the hydrodynamic stresses exerted by the fluid within the tube, and equal to

$$[p - 2\mu \partial v / \partial r]_{r=a} \quad \text{and} \quad -\mu [\partial u / \partial r + \partial v / \partial x]_{r=a}$$

in the  $r$ - and  $x$ -direction, respectively, where  $(u, v, 0)$  is the fluid velocity vector, and  $p$  is the fluid pressure perturbation. (ii) There are also tethering stresses exerted by the material outside the tube.

We model these (following Patel & Fry, 1966) by supposing that the external tissue provides added inertia, stiffness and (viscoelastic) damping. Thus we take

$$\left. \begin{aligned} X &= -\mu \left[ \frac{\partial u}{\partial r} + \frac{\partial v}{\partial x} \right]_{r=a} - M_1 \frac{\partial^2 \xi}{\partial t^2} - L_1 \frac{\partial \xi}{\partial t} - K_1 \xi, \\ Y &= \left[ p - 2\mu \frac{\partial v}{\partial r} \right]_{r=a} - M_2 \frac{\partial^2 \eta}{\partial t^2} - L_2 \frac{\partial \eta}{\partial t} - K_2 \eta. \end{aligned} \right\} \quad (2.28)$$

*Equations of motion and kinematic boundary conditions for the fluid*

The linearised axial and radial momentum equations are

$$\left. \begin{aligned} \frac{\partial u}{\partial t} &= -\frac{1}{\rho} \frac{\partial p}{\partial x} + \nu \left( \frac{\partial^2 u}{\partial r^2} + \frac{1}{r} \frac{\partial u}{\partial r} + \frac{\partial^2 u}{\partial x^2} \right), \\ \frac{\partial v}{\partial t} &= -\frac{1}{\rho} \frac{\partial p}{\partial r} + \nu \left( \frac{\partial^2 v}{\partial r^2} + \frac{1}{r} \frac{\partial v}{\partial r} - \frac{v}{r^2} + \frac{\partial^2 v}{\partial x^2} \right), \end{aligned} \right\} \quad (2.29)$$

while the continuity equation is

$$\frac{1}{r} \frac{\partial}{\partial r} (rv) + \frac{\partial u}{\partial x} = 0. \quad (2.30)$$

The linearised kinematic boundary conditions at the wall are

$$u|_{r=a} = \frac{\partial \xi}{\partial t}, \quad v|_{r=a} = \frac{\partial \eta}{\partial t}, \quad (2.31)$$

while on the axis we have

$$v = \frac{\partial u}{\partial r} = 0 \quad \text{on} \quad r = 0. \quad (2.32)$$

### Statics

In static experiments to measure the elastic properties of excised blood vessels, it is usual to define 'incremental' values of the elastic parameters (§ 1.1). An incremental value for  $B_{11}$ , for example, would be equal to  $a$  times the increment of circumferential tension,  $t'$ , for unit increment in radial strain,  $\eta$ , longitudinal strain being zero (see the first of equations (2.26)). Consider an experiment, therefore, in which  $\xi$  is held to zero and an increase in internal pressure,  $p$ , is applied. Then (2.25) and (2.26), with (2.28) in which

radial tethering is absent, lead to

$$pa = [(B_{11} - T)/a]\eta.$$

Thus the incremental value of  $B_{11}$  is in fact  $(B_{11} - T)$ , and it is this value that is measured, and through (2.27) related to incremental Young's modulus, etc.

We find similarly, by considering an experiment in which  $p$  remains zero, but a small extra longitudinal stress  $\Delta X$  is applied to the artery, that

$$[B_{22} - B_{12}(B_{21} + S - T)/(B_{11} - T)] \partial^2 \xi / \partial x^2 = -\Delta X,$$

while if  $\eta$  could be held zero we would have

$$B_{22} \partial^2 \xi / \partial x^2 = -\Delta X, \quad (B_{12}/a) \partial \xi / \partial x = p.$$

Thus it is clear that the incremental value of  $B_{21}$  is  $B_{21} + S - T$ , while  $B_{12}$  and  $B_{22}$  are unchanged. For a full discussion of the experiments needed to measure the incremental values of  $B_{11}$ ,  $B_{21}$  etc., see Patel & Vaishnav (1972).

### *Dispersion relation*

The problem is now completely specified. We reduce it to one in which only ordinary differential equations have to be solved by supposing every variable to be proportional to  $e^{i\omega(t-x/c)}$ , where  $\omega$  is the real angular frequency and  $c$  is the complex wave speed. We denote the corresponding amplitude of every quantity by the suffix 1. The linearisation of the fluid mechanical equations is valid as long as

$$|u_1/c| \ll 1 \tag{2.33}$$

always; the linearisation of the elasticity requires

$$|\eta_1/a| \ll 1 \quad \text{and} \quad |\xi_1/a| \ll 1,$$

which are both equivalent to (2.33) from the kinematic boundary conditions (2.31), together with the continuity equation (2.30). We simplify the equations even further by making the long-wavelength approximation,  $|\omega a/c| \ll 1$ , which is certainly valid *in vivo* (rather more so than the linearity approximation), and which means that (a) the  $\partial^2/\partial x^2$  terms on the right-hand sides of (2.29) are negligible, (b) the second of equations (2.29) reduces to  $\partial p_1/\partial r = 0$ , and (c) the

second term in each square bracket in (2.28) is much less than the first. This assumption is not a necessary condition for solving the equations, but it makes the solution less cumbersome.

The first of equations (2.29) now reduces to Bessel's equation, and the solution satisfying the boundary condition at  $r = 0$  is

$$u_1(r) = (p_1/\rho c_0)[c_0/c + AJ_0(i^{3/2}\alpha r/a)/J_0(i^{3/2}\alpha)], \quad (2.34)$$

where  $c_0$  is a scale for  $c$ , which can conveniently be taken equal to the Moens-Korteweg speed (see (2.7a)),  $A$  is an as yet undetermined constant, and  $\alpha$  is the *Womersley parameter* (Womersley, 1955):

$$\alpha = a(\omega/\nu)^{1/2}, \quad (2.35)$$

Equation (2.30) then yields

$$v_1(r) = \frac{i\omega a p_1}{c_0^2 \rho} \cdot \frac{c_0}{c} \left[ \frac{c_0}{c} \cdot \frac{r}{2a} + \frac{AJ_1(i^{3/2}\alpha r/a)}{i^{3/2}\alpha J_0(i^{3/2}\alpha)} \right].$$

The four unknowns  $\xi_1$ ,  $\eta_1$ ,  $p_1$  and  $p_1 A$  now satisfy four homogeneous equations: the two equations (2.31) and the two equations (2.25), using (2.26) and (2.28), reduce respectively to

$$\left. \begin{aligned} (k' + A)(ap_1/\rho c_0^2) &= i(\omega a/c_0)\xi_1, \\ (k'^2 + k'FA)(ap_1/\rho c_0^2) &= 2\eta_1, \\ \left( B'_{22}k'^2 + \frac{K'_1}{(\omega^2 a^2/c_0^2)} \right) \left( \frac{\omega a}{c_0} \xi_1 \right) + ik'B'_{21}\eta_1 + \frac{iF}{2} \left( \frac{ap_1 A}{\rho c_0^2} \right) &= 0, \\ -ik'B'_{12}(\omega a/c_0)\xi_1 + (B'_{11} + K'_2)\eta_1 - ap_1/\rho c_0^2 &= 0. \end{aligned} \right\} \quad (2.36)$$

Various complex dimensionless parameters have been used here:

$$k' = \frac{c_0}{c}, \quad K'_j = \frac{a}{\rho c_0^2} [K_j + i\omega L_j - \omega^2(M_j + \rho_w h)] \quad (j = 1, 2),$$

$$B'_{11} = \frac{B_{11} - T}{\rho a c_0^2}, \quad B'_{12} = \frac{B_{12}}{\rho a c_0^2},$$

$$B'_{21} = \frac{B_{21} - T + S}{\rho a c_0^2}, \quad B'_{22} = \frac{B_{22}}{\rho a c_0^2},$$

and

$$F(\alpha) = 2J_1(i^{3/2}\alpha)/i^{3/2}\alpha J_0(i^{3/2}\alpha). \quad (2.37)$$

The four equations (2.36) have a solution only if the quantity  $k'^2$  satisfies the quadratic equation

$$k'^4(1-F)[B'_{22}(B'_{11}+K'_2)-B'_{12}B'_{21}] + k'^2\{F(B'_{12}+B'_{21}-\frac{1}{2}B'_{11}-\frac{1}{2}K'_2)-2B'_{22} + [K'_1/(\omega^2 a^2/c_0^2)](B'_{11}+K'_2)(1-F)\} + F - 2K'_1/(\omega^2 a^2/c_0^2) = 0. \quad (2.38)$$

This dispersion relation has two roots for  $k'^2$ , indicating the existence of two types of wave, only one of which will be the pressure wave analysed one-dimensionally in § 2.1. Note that if  $k' = k'_r + ik'_i$  (where  $k'_r$  is always chosen to be  $>0$ ), the speed of propagation of the wave is  $c_0/k'_r$  and its attenuation constant  $k$  from (2.8), is given by

$$k = -2\pi k'_i/k'_r, \quad (2.39)$$

so the imaginary part of  $k'$  must be negative for attenuation. Atabek (1968) calls  $e^{-k}$  the 'transmission per wavelength'. To investigate the character of the waves whose dispersion relation is (2.38), we examine various particular cases.

In all cases, the solution will depend on the value of  $\alpha$  through the function  $F(\alpha)$ , from (2.37). The quantity  $\alpha$  is defined in (2.35), and can be interpreted physically in various ways. The ratio of tube radius to the thickness of the oscillatory (Stokes) boundary layer on the tube wall is proportional to  $\alpha$ . When  $\alpha$  is large, the boundary layer is thin and the velocity profile effectively flat across the core (this follows from the expression (2.34) for  $u_1(r)$ , since, as  $y \rightarrow \infty$ ,

$$J_0(i^{3/2}y) \sim \frac{e^{y/\sqrt{2}}}{\sqrt{2\pi y}} \exp\left\{i\left(\frac{y}{\sqrt{2}} - \frac{\pi}{8}\right)\left[1 + O\left(\frac{1}{y}\right)\right]\right\},$$

so that

$$1 - \frac{u_1(r)}{u_1(0)} \sim \frac{A}{k'} \left(\frac{a}{r}\right)^{1/2} \exp\left[-\frac{\alpha}{\sqrt{2}}(1+i)(1-r/a)\right]$$

as  $\alpha \rightarrow \infty$ , which is familiar as the Stokes layer profile). When  $\alpha$  is small, the tube is fully occupied by the innermost portion of the boundary layer, and the flow is quasi-steady ( $J_0(z) \sim 1 - \frac{1}{4}z^2$  as  $|z| \rightarrow 0$ , so

$$u_1(r) \propto k' + A[1 - i(\alpha^2/4)(1 - r^2/a^2)]$$

as  $\alpha \rightarrow 0$ , which is a constant plus Poiseuille flow).  $\alpha^2$  can also be thought of as the ratio between the viscous diffusion time and the period of the oscillation, or as an unsteady Reynolds number. The asymptotic expansions of  $F(\alpha)$  at large and small values of  $\alpha$  are

$$\begin{aligned} F(\alpha) &\sim (2/\alpha i^{1/2})[1 + (1/2\alpha) + O(\alpha^{-2})] \quad \text{as } \alpha \rightarrow \infty \\ &\sim 1 - i(\alpha^2/8) - (\alpha^4/48) + O(\alpha^6) \quad \text{as } \alpha \rightarrow 0. \end{aligned}$$

In large arteries  $\alpha$  is large (see § 1.2): in the aorta,  $\alpha \approx 13$  (dog) and 17 (man). For a heart-rate of 2 Hz,  $\alpha$  would be approximately 1 in a vessel of diameter 0.03 cm;  $\alpha \ll 1$  in the microcirculation (vessels  $< 0.01$  cm in diameter).

### 2.2.1 *Isotropic, elastic walls; no wall inertia, no initial stresses, no tethering*

Here  $S = T = K'_1 = K'_2 = 0$ ,  $B_{11} = B_{22} = B$  (say), which is real, and  $B'_{12} = B'_{21} = \sigma B$ . Furthermore, the Moens–Korteweg wave speed  $c_0$  is given by

$$c_0^2 = Eh/2\rho a = B(1 - \sigma^2)/2\rho a,$$

so (2.38) reduces to

$$(1 - \sigma^2)F - [4 + F(1 - 4\sigma)]k'^2 + 4(1 - F)k'^4 = 0. \quad (2.40)$$

We can also set  $\sigma = \frac{1}{2}$  for incompressible material. The solutions of (2.40) are complex and depend on  $\alpha$  through  $F(\alpha)$ , from (2.37).

$\alpha \rightarrow \infty$

As  $\alpha \rightarrow \infty$ , the two roots of (2.40) are approximately

$$k'^2 = 1 + \frac{9}{8\alpha i^{1/2}} \quad \text{and} \quad k'^2 = \frac{3}{8\alpha i^{1/2}} \left[ 1 + \frac{1}{2\alpha} \left( 1 + \frac{7}{4i^{1/2}} \right) \right];$$

the former represents the Moens–Korteweg wave (speed  $c_0$ ) with little attenuation ( $k \approx 9\pi/8\sqrt{2}\alpha \approx 2.5/\alpha$ ; see (2.39)), and the latter a much faster wave with speed  $c_0(8\alpha/3)^{1/2} \sec \frac{1}{8}\pi$  and attenuation constant  $k \approx 2\pi \tan \frac{1}{8}\pi \approx 2.6$  reflecting a constant attenuation of 93% per wavelength. However, since the speed of this wave is so

large, the wavelength is also large, and the attenuation per Moens-Korteweg wavelength would be only 34% for  $\alpha = 13$ .

It is interesting to note that, for the first type of wave, a frequency of 40 Hz leads to a value of  $\alpha$  of about 60, and hence to a value of  $k \approx 0.04$ . This is not adequate to make up the difference between the value predicted from observed viscoelastic wall properties, (2.9), and the observed value of  $k (=0.7-1.0)$ , although its small magnitude may explain why Anliker *et al.* (1968*a*) did not observe the frequency-dependence of attenuation predicted here, while McDonald & Gessner (1968) did observe it at somewhat lower frequencies (up to 20 Hz). Note that for  $\alpha = 13$  (dog's aorta)  $k \approx 0.19$ , which is not negligibly small. Note too that the wave speed is predicted to be slightly frequency-dependent, since  $c_0/k'_r \approx c_0(1 - 9/8\alpha\sqrt{2})$ ; however, the amount of dispersion predicted for  $\alpha \geq 60$  is negligible, and Anliker *et al.* (1968*a*) observed no dispersion at such high frequencies.

The nature of the two types of wave can be determined by solving equations (2.36) for the unknown coefficients. From them we deduce that, when  $k' = 1$ ,

$$\eta_1 = \frac{1}{2}ap/\rho c_0^2, \quad (\omega/c_0)\xi_1 = i\eta_1/2a,$$

while when  $k' = (3/8\alpha)^{1/2} e^{-i\pi/8}$ ,

$$\eta_1 = \frac{3}{16\alpha i^{1/2}} \cdot \frac{ap_1}{\rho c_0^2}, \quad \frac{\omega}{c_0}\xi_1 = \left(\frac{2\alpha}{3}\right)^{1/2} \frac{i^{5/4}}{a} \eta_1.$$

In the first type of wave, the radial wall displacements are in phase with the pressure pulsations, and the longitudinal wall displacements are (when appropriately non-dimensionalised) of the same order of magnitude as the radial displacements, with a  $90^\circ$  phase lead. This is just what one would expect for the pressure wave analysed in § 2.1. For the second type of wave, however, the radial displacement is much smaller for the same pressure amplitude, and the longitudinal displacements are much larger than the radial. Thus this is a shear wave, in which the principal wall oscillations are longitudinal, and the (small) inertia is provided by the fluid dragged back and forth in the Stokes boundary layers (obviously wall inertia would eventually limit the wave speed as  $\alpha \rightarrow \infty$ ).

$\alpha \rightarrow 0$

In this limit, the roots of (2.40) are approximately

$$k'^2 = \frac{6}{i\alpha^2} \left( 1 + \frac{i\alpha^2}{6} \right) \quad \text{and} \quad k'^2 = \frac{1}{4} \left( 1 - \frac{i\alpha^2}{8} \right).$$

The former represents the pressure wave, with a low propagation speed of  $c_0\alpha/\sqrt{3}$  and attenuation per (very short) wavelength given by  $k = 2\pi$ . The latter represents the shear wave, with a finite wave speed  $2c_0$  in this limit, and negligible attenuation, which seems rather surprising until we recognise that the fluid in the tube is carried bodily along with the longitudinal wall motions and the shear-rate within it is negligible. The slowly propagating pressure wave is not really a wave at all in this limit, since inertia is negligible. There is, instead, a balance between the elastic restoring forces and viscosity, which is a diffusive process rather than a wave (see Lighthill's appendix to Caro, Foley & Sudlow (1970)), and this is the mechanism governing the transmission of the pressure pulse through the microcirculation.

Computations for intermediate values of  $\alpha$  were made for the pressure wave by Womersley (1957), and for the longitudinal wave by other authors, e.g. Atabek (1968). The results show continuous, smooth variation of wave speed and attenuation between  $\alpha = 0$  and  $\alpha = \infty$ , for each type of wave. The wave speed in each case increases monotonically with  $\alpha$ , as does the factor  $e^{-k}$  for the pressure waves, although for the longitudinal waves  $e^{-k}$  has a minimum at  $\alpha \approx 3$  (Atabek, 1968), at least when some wall inertia is present.

Womersley (1957) ignored the existence of the fast shear waves, although the second solution for  $k'^2$  would have arisen from his theory. The reason must be that significant longitudinal wall motions are not observed in real arteries, so no such waves could be measured. The absence of shear waves can be directly attributed to longitudinal wall tethering, as we proceed to show.

### 2.2.2 *The effect of longitudinal tethering*

As a preliminary to assessing the effects of the different parameters in (2.38), an estimate of their approximate value in normal arteries will be obtained. We know that the Moens–Korteweg wave speed  $c_0$



is given by

$$c_0^2 = E_\theta h / 2\rho a$$

when  $E_\theta$  is real; using this relation in equations (2.37) for  $B'_{11}$  (incremental) etc. leads to

$$\begin{aligned} B'_{11} &= \frac{2}{1 - \sigma_\theta \sigma_x}, & B'_{12} &= \frac{2\sigma_x}{1 - \sigma_\theta \sigma_x}, \\ B'_{21} &= \frac{2\sigma_\theta E_x / E_\theta}{1 - \sigma_\theta \sigma_x}, & B'_{22} &= \frac{2E_x / E_\theta}{1 - \sigma_\theta \sigma_x}. \end{aligned}$$

These quantities are all of order 1: if we take  $E_x/E_\theta = 1.2$  and  $\sigma_\theta = \sigma_x = 0.29$  (cf. Patel & Vaishnav, 1972), we obtain

$$B'_{11} = 2.18, \quad B'_{12} = 0.63, \quad B'_{21} = 0.76, \quad B'_{22} = 2.62.$$

Patel & Vaishnav (1972) also give values for the tethering constants  $K_{1,2}$ ,  $L_{1,2}$ ,  $M_{1,2}$  in the aorta. They suggest that the radial and longitudinal tethering constants are roughly equal, and give

$$\begin{aligned} K_{1,2} &\approx 33 \text{ kN m}^{-2} (\text{m})^{-1}, & L_{1,2} &\approx 17 \text{ kN m}^{-2} (\text{m s}^{-1})^{-1}, \\ M_{1,2} + \rho_w h &\approx 4 \text{ N m}^{-2} (\text{m s}^{-2})^{-1}; \end{aligned}$$

thus the inertia terms are negligibly small except at extremely high frequencies ( $\omega \sim 10^2 \text{ s}^{-1}$ ), and

$$K'_{1,2} \approx (33 + 17i\omega)(a/\rho c_0^2) \times 10^3.$$

Now in the aorta,  $a \approx 10^{-2} \text{ m}$ ,  $c_0 \approx 5 \text{ m s}^{-1}$  and  $\rho = 10^3 \text{ kg m}^{-3}$ , so  $|K'_{1,2}| \approx 0.9$  when  $\omega = 4\pi \text{ s}^{-1}$ , which is markedly smaller than  $B'_{11}$  or  $B'_{22}$ , so that the terms involving  $K'_2$  in (2.38) can be neglected. However, the terms involving  $K'_1$  are divided by  $\omega^2 a^2 / c_0^2$ , which is very small, about  $6.3 \times 10^{-4}$  for  $\omega = 4\pi$ . Thus  $|K'_1|/(\omega^2 a^2 / c_0^2) \approx 140$ , which is much larger than the other terms, and longitudinal tethering is dominant. Equation (2.38) now reduces approximately to

$$\beta_1 k'^4 + \{\beta_2 K - [\beta_3 / (1 - F)]\} k'^2 - [2K / (1 - F)] = 0, \quad (2.41)$$

where

$$\begin{aligned} \beta_1 &= B'_{22} B'_{11} - B'_{12} B'_{21}, & \beta_2 &= B'_{11}, \\ \beta_3 &= -F(B'_{12} + B'_{21} - \tfrac{1}{2} B'_{11}) + 2B'_{22}, \end{aligned}$$

and

$$K = K'_1 / (\omega^2 a^2 / c_0^2)$$

so that  $|K| \gg 1$ . The second term in the square brackets is negligible unless  $\alpha$  is very small when  $1 - F \sim \frac{1}{8}\alpha^2$ .

When  $\alpha$  is not small, so that  $1 - F = O(1)$ , the two solutions of (2.41) are approximately

$$k'^2 = 2/(1 - F)\beta_2 \quad \text{and} \quad k'^2 = -\beta_2 K/\beta_1. \quad (2.42)$$

The first of these represents the pressure wave, as we can see by putting  $F = 0$  ( $\alpha \rightarrow \infty$ ) and  $\beta_2 = B'_{11} = 2/(1 - \sigma^2)$  for an isotropic elastic solid. Then  $k'^2 = 1 - \sigma^2$  and  $c^2 = c_0^2/(1 - \sigma^2)$ . This is just the result obtained in an elastic tube when longitudinal wall motions are completely prevented (cf. (2.7b) and Lighthill (1975), chapter 12). Indeed, letting  $K \rightarrow \infty$  directly in equations (2.36) (with  $F \neq 0$ , necessarily) shows at once that a consistent solution is one in which

$$\xi_1 \approx 0, \quad B'_{11}\eta_1 \approx ap_1/\rho c_0^2, \quad A \approx -k', \quad k'^2 = 2/(1 - F)\beta_2. \quad (2.43)$$

Thus the phase of  $\eta$  differs from that of  $p$  only through the complex nature of the distensibility, proportional to  $B'_{11}^{-1}$ . Also the velocity profile (2.34) reduces to

$$u_1(r) = (p_1/\rho c_0)k'[1 - J_0(i^{3/2}\alpha r/a)/J_0(i^{3/2}\alpha)]; \quad (2.44)$$

this is precisely the velocity profile driven by an oscillatory pressure gradient in a *rigid* tube (Womersley, 1955), as we would expect for long waves in which there is no longitudinal wall motion. Only the amplitude and phase depend on wall distensibility and viscoelasticity through the factor  $k'$ .

The second of the solutions (2.42) represents the longitudinal wave, but it is no longer necessarily a fast wave, as we can see if we put

$$-iK = (1/\rho a \omega^2)(\omega L_1 - iK_1) = M e^{-i\chi}.$$

Therefore, neglecting for now the fact that  $\beta_1$  and  $\beta_2$  are complex, we have the speed of propagation equal to

$$c_0/k'_r = c_0(\beta_1/\beta_2 M)^{1/2} \sec(\frac{1}{2}\chi + \frac{1}{4}\pi). \quad (2.45)$$

In general this is very small because  $M = |K|$  is very large, but if  $\chi$  is close to  $\frac{1}{2}\pi$ , i.e. if  $K_1 \gg \omega L_1$ , the speed would become large. This is to be expected since increasing the elastic restoring force while keeping the viscous damping force constant should increase the

wave speed. For the numbers quoted above,  $K_1/L_1 \approx 2$ , so  $\omega L_1$  will exceed  $K_1$  for frequencies greater than  $1/\pi$ , and the  $M^{-1/2}$  factor in (2.45) will dominate. These longitudinal waves are attenuated by a factor  $e^{-k}$  per wavelength, where

$$k = 2\pi \tan\left(\frac{1}{2}\chi + \frac{1}{4}\pi\right),$$

which is significantly greater than  $2\pi$ , and increases as  $\chi$  increases, i.e. as the elastic tethering constant,  $K_1$ , increases relative to the viscous constant,  $\omega L_1$ . The purely numerical results of Atabek (1968) are consistent with this result. Since the wave speed and hence wavelength are in general small, the attenuation per unit distance will be extremely great; this is no doubt why such waves are not normally observed, at least in the aorta and femoral arteries. Anliker *et al.* (1968*b*), however, generated high-frequency axial waves in the exposed canine *carotid* artery, and observed wave speeds of about three times  $c_0$  (with attenuation per wavelength about three times that of the pressure wave); the reason  $c_0$  is not small is presumably because the exposed carotid artery is not tethered, with the consequence that  $M$  is not large and the visco-elastic properties of the artery wall itself are once more important.

If  $\alpha$  is small enough for  $1/\alpha^2$  to be large compared with  $K$ , the roots of (2.41) reduce to

$$k'^2 = 8\beta_3/\alpha^2\beta_1 \quad \text{and} \quad k'^2 = -2K/\beta_3. \quad (2.46)$$

The former has a very low wave speed, and this and the attenuation per wavelength are independent of the tethering constants; this represents the pressure 'wave', as in the absence of tethering. The latter represents the longitudinal wave, and its properties are again dominated by the tethering constants.

### 2.2.3 The physiological pressure pulse (summary)

Longitudinal tethering prevents axial wall movements, and causes the physiological pressure wave to satisfy equations (2.43), with a rigid-tube velocity profile (2.44). The quantity  $\beta_2$  is complex, equal to

$$B'_{11} = (E_{\theta\text{dyn}} + i\eta\omega)h/\rho\alpha c_0^2(1 - \sigma_\theta\sigma_x),$$

and  $c_0$  is best defined as the speed of propagation, in the absence of tethering, as  $\alpha \rightarrow \infty$ ; i.e. as

$$c_0 = |E_{\theta \text{ dyn}} + i\eta\omega|^2 h / E_{\theta \text{ dyn}} 2\rho a. \quad (2.47a)$$

Thus the value of  $k'^2$  is

$$k'^2 = \frac{(1 - \sigma_\theta \sigma_x)}{1 - (2/\alpha i)^{1/2}} (1 - i \tan \theta), \quad (2.47b)$$

where  $\tan \theta = \eta\omega / E_{\theta \text{ dyn}}$ , from (2.9), which has a value of about  $\frac{1}{6}$ . The feature of this result that has not yet been discussed is the fact that  $\sigma_\theta$  and  $\sigma_x$  are complex. Patel *et al.* (1973) measured the dynamic anisotropic elastic properties of the canine aorta, and obtained

$$\sigma_\theta \approx 0.28 + 0.07i, \quad \sigma_x \approx 0.16 + 0.02i,$$

so that the factor

$$(1 - \sigma_\theta \sigma_x) \approx 0.91 - 0.03i.$$

This means (a) that the wave speed  $c_0/k'_r$  is increased above  $c_0$ , but by a smaller factor than when  $\sigma_\theta = \sigma_x = 0.5$ , and (b) that the complex Poisson's ratios have a negligible influence on the damping, all of which must come from the complex Young's moduli of the wall, at least for high-frequency waves when  $\alpha$  is very large as in the experiments of Anliker *et al.* (1968a).

#### 2.2.4 Flow-rate and wall shear

As was explained in § 1.2, two aspects of the velocity field are of particular interest. One is the volume flow-rate,

$$Q = \int_0^a 2\pi r u \, dr,$$

and the other is the shear stress on the wall,

$$\tau = -\mu \left. \frac{\partial u}{\partial r} \right|_{r=a}$$

When the velocity profile is given by the rigid-tube equation, (2.44), for a pressure-wave amplitude of  $p_1$ , the complex amplitudes of these quantities turn out to be

$$Q_1 = (\pi a^2 p_1 / \rho c_0) k' (1 - F) \quad (2.48)$$

and

$$\tau_1 = (\nu p_1 / ac_0) k' \cdot \frac{1}{2} i \alpha^2 F. \quad (2.49)$$

In these equations  $k'/c_0 = 1/c$ , and  $-i\omega p_1/c$  is the (complex) pressure-gradient amplitude, which we may denote by  $-G_1$ . For large and small values of  $\alpha$ , (2.48) and (2.49) become

$$\left. \begin{aligned} Q_1 &\sim (-\pi a^2 / \rho \omega) G_1 i (1 - 2/\alpha i^{1/2}) \\ \tau_1 &\sim (-\nu / a \omega) G_1 i^{3/2} \alpha (1 + 1/2\alpha) \end{aligned} \right\} \text{as } \alpha \rightarrow \infty, \quad (2.50)$$

and

$$\left. \begin{aligned} Q_1 &\sim (\pi a^2 / \rho \omega) G_1 (\alpha^2 / 8) (1 - i \alpha^2 / 6) \\ \tau_1 &\sim (-\nu / a \omega) G_1 (i \alpha^2 / 2) (1 - i \alpha^2 / 8) \end{aligned} \right\} \text{as } \alpha \rightarrow 0. \quad (2.51)$$

As Lighthill (1975) has pointed out, good accuracy is achieved by using (2.50) for  $\alpha > 4$  and (2.51) for  $\alpha < 4$ . Note that the amplitude of the centre-line velocity,  $u_1(0)$ , differs from that of the average velocity,  $Q/\pi a^2$ , by a factor  $[1 - 1/J_0(i^{3/2}\alpha)]/(1 - F)$ , which is close to 1 for large  $\alpha$ , and close to 2 for small  $\alpha$ , when the flow is approximately Poiseuille flow. Note too that at large  $\alpha$ , the flow-rate is  $\frac{1}{2}\pi$  out of phase with the pressure gradient, as one would expect for an inviscid fluid (§ 2.1). At very small  $\alpha$  on the other hand, the flow-rate is in phase with the pressure gradient, since the flow is quasi-steady.

Womersley and McDonald verified the validity of using the rigid-tube velocity profiles in practice by measuring the pressure-gradient waveform (in a dog's femoral artery), performing a Fourier analysis on it, using equation (2.48) to calculate  $Q$  for each term (with  $c_0/k' = c$  assumed real), and then recombining the answers to obtain a predicted flow-rate waveform. They compared the results with the actual flow-rate waveform, measured directly with an electromagnetic flowmeter. Agreement was very good, as shown in fig. 2.5 (see McDonald, 1974, p. 130).

The results of this section have confirmed the validity of the one-dimensional wave theory presented in § 2.1 to describe linear pressure waves in arteries, as long as for each frequency the wave speed  $c_0$  is replaced by  $c_0/k'_r$  ( $k'_r$  given by (2.47*b*)) and the flow-rate is related to the pressure by (2.48) instead of

$$Q_1 = \pi a^2 p_1 / \rho c_0 = (A/\rho c_0) p_1, \quad (2.52)$$

as predicted by the theory of § 2.1. The quantity  $Q_1/p_1$  is called the characteristic *admittance* of the tube. In the high-frequency limit

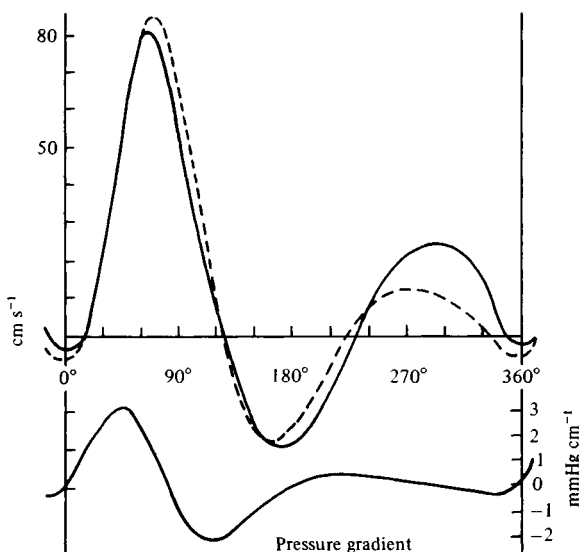


Fig. 2.5. Waveforms of average velocity (upper traces) in a dog's femoral artery; continuous curve, measured with an electromagnetic cuff flowmeter; broken curve, calculated from the measured pressure gradient (lower trace) according to Womersley's rigid-tube theory. (After McDonald, 1974.)

this is equal to  $A/\rho c_0$ , which is independent of frequency. In this case it is relatively simple to take non-linearities into account by a one-dimensional theory, as shown in § 2.1. At lower frequencies, however, the dispersion of the wave makes non-linear theory more difficult. Womersley (1957) extended his two-dimensional theory to second order in wave amplitude, to take account of small non-linearities. The resulting combinations of Fourier modes became very complicated. Olsen & Shapiro (1967) developed the one-dimensional theory in powers of wave amplitude, and showed, by comparison with model experiments in rubber tubes, that the second-order results were accurate enough to cover normal physiological events. All these theories confirm that the *normal* pressure wave in arteries can be treated as approximately linear.

### 2.3 Effects of taper and branchings (linear theory)

The theory presented so far is adequate for uniform viscoelastic tubes, but is inadequate for real arteries because they are not

uniform. They suffer both from a continuous variation in cross-sectional area and distensibility, and from repeated branchings. In this section we show to what extent the one-dimensional linear theory can be adapted to cope with such non-uniformities. There is little in this section that has not already been outlined by Lighthill (1975).

### 2.3.1 *Taper*

If the rate of change of wall properties with distance along the tube is sufficiently gradual, i.e. takes place over a length-scale large compared with the wavelength of the wave, then the modification of a wave as it travels along the tube can be analysed by the WKB-method (Cole, 1968), first applied to arteries by Taylor (1965). Furthermore if, as in arteries, the wavelength is long compared with the tube radius, and if linear theory is applicable, the one-dimensional equations governing the wave, from (2.1)–(2.3), are

$$\left. \begin{aligned} \partial Q / \partial x + (Y/c) \partial p / \partial t &= 0, \\ \partial Q / \partial t + c Y (\partial p / \partial x) &= 0, \end{aligned} \right\} \quad (2.53)$$

where  $Q = Au$  is the volume flow-rate and  $Y = A/\rho c$  is the characteristic admittance of the tube, which, with the wave speed  $c$ , may be complex, but is only weakly frequency-dependent. We assume that both  $c$  and  $Y$  are slowly varying functions of  $x$ , and introduce a new variable  $\tilde{x} = \varepsilon x$  ( $\varepsilon \ll 1$ ) so that  $c$  and  $Y$  are functions only of  $\tilde{x}$ . We shall seek an asymptotic expansion of the solution of (2.53) that is uniformly valid for all  $x$  and  $t$  as  $\varepsilon \rightarrow 0$ , and present the theory in such a way that subsequent terms in the expansion can be readily constructed, in principle.

The equations (2.53) can be combined into the following single equation for  $p$ :

$$\frac{1}{c^2} \frac{\partial^2 p}{\partial t^2} = \frac{\partial^2 p}{\partial x^2} + \frac{\varepsilon (cY)'}{cY} \frac{\partial p}{\partial x},$$

where a prime denotes differentiation with respect to  $\tilde{x}$ , the 'slow' variable. We introduce a new 'fast' variable

$$x_1 = \int_0^x \frac{dx}{c(\varepsilon x)},$$

in terms of which the equation for  $p$  is

$$\frac{\partial^2 p}{\partial t^2} = \frac{\partial^2 p}{\partial x_1^2} - \varepsilon c' \frac{\partial p}{\partial x_1} + \frac{\varepsilon (cY)'}{Y} \frac{\partial p}{\partial x_1}. \quad (2.54)$$

Now suppose  $p$  is expanded in a power series:

$$p(x_1, t, \tilde{x}, \varepsilon) = p_0(x_1, t, \tilde{x}) + \varepsilon p_1(x_1, t, \tilde{x}) + \cdots.$$

Substitute into (2.54) and equate like powers of  $\varepsilon$ . The zeroth-order equation is

$$\partial^2 p_0 / \partial t^2 - \partial^2 p_0 / \partial x_1^2 = 0,$$

so

$$p_0 = B(\tilde{x})f(t - x_1)$$

for waves travelling in the positive- $x$  direction, where  $f$  is arbitrary (depending on initial conditions) and  $B(\tilde{x})$  is an as yet undefined function. The first-order equation is

$$\begin{aligned} \frac{\partial^2 p_1}{\partial t^2} - \frac{\partial^2 p_1}{\partial x_1^2} &= 2c \frac{\partial^2 p_0}{\partial \tilde{x} \partial x_1} - c' \frac{\partial p_0}{\partial x_1} + \frac{(cY)'}{Y} \frac{\partial p_0}{\partial x_1} \\ &= f'(t - x_1)[-2cB' + c'B' - (cY)'B/Y]. \end{aligned}$$

Now  $f'(t - x_1)$  will, in general, be an oscillatory function, so that the solution for  $p_1$  will exhibit resonance and hence no longer be small, unless the term in the square brackets is identically zero. In order that the proposed expansion be uniformly valid, we therefore require that this bracket is identically zero, which determines  $B$ . In fact we obtain

$$B(\tilde{x})/B(0) = [Y(0)/Y(\tilde{x})]^{1/2},$$

and the final zeroth-order solution for  $p$  (in terms of the old  $x$ -variable) is

$$p = \left[ \frac{Y(0)}{Y(x)} \right]^{1/2} f\left(t - \int_0^x c^{-1} dx\right). \quad (2.55)$$

The corresponding solution for  $Q$ , from either of equations (2.53), is

$$Q = Y(x)p. \quad (2.56)$$



These results show that, at every location along the slowly varying tube, the flow-rate is equal to the *local* characteristic admittance multiplied by the pressure, but the inverse of the wave speed is equal to the *average* value of the characteristic inverse wave speed over the length of tube traversed by the wave. In arteries,  $|c|$  increases with distance from the heart, while  $A$ , and hence  $|Y|$ , decreases. Thus the amplitude of the pressure pulse will increase ( $\propto |Y|^{-1/2}$ ) while that of the flow-rate pulse will decrease ( $\propto |Y|^{1/2}$ ). Furthermore, the magnitude of the (complex) wave speed will not be as large as would be expected from purely local measurements of distensibility.

The above theory is very attractive, but unfortunately cannot be applied directly to the pressure pulse generated by the heart in mammalian arteries. This is because of the requirement that the length-scale of tube variation should be large compared with the wavelength, whereas we have already seen that the wavelength of the fundamental wave (frequency = heart-rate  $\approx 2$  Hz in dogs) is several metres, while the length of the longest vessel, the aorta, is of the order of half a metre. The qualitative agreement between the predicted peaking of the pressure pulse (and the corresponding decrease in flow-rate amplitude) and the observations (fig. 1.14) can be no more than suggestive.

The theory should, however, be more applicable to experiments such as those of Anliker *et al.* (1968*a*) and of Hstand & Anliker (1973), in which high-frequency waves are generated at one location in an artery and measured at another. The frequency range used was 40–120 Hz, so the wavelength would have been between 4 and 12 cm in the aorta, which is reasonably small compared with the length of that vessel. The ratio between the amplitude of the pressure wave at one position,  $x$ , compared with that at another position closer to the origin of the wave, 0, is predicted to be

$$\left[ \frac{Y(0)}{Y(x)} \right]^{1/2} \exp \left( \omega \int_0^x \frac{k'_1}{c_0} dx \right), \quad (2.57)$$

where  $c_0$  and  $k' (= k'_r + ik'_i)$  are given by (2.47*a, b*) in which the  $1/\alpha$  term is negligible. Hstand & Anliker (1973) fitted their measurements in the aorta to the curve  $e^{-kx/\lambda}$ , where  $\lambda$  is the wavelength, and found  $k = 0.7$ – $1.0$  for waves propagated peripherally and

$k = 1.3$ – $1.5$  for waves propagated centrally. Values of  $x$  of about 5 cm were generally used. If we assume that the ratio of the viscous to the elastic components of the distensibility (i.e.  $\tan \theta$ ) remains roughly uniform, then the contribution to  $k$  from the integral in (2.57) will be approximately the same for both peripheral and central waves, and equal to

$$2\pi \int_0^x \frac{E_\theta^{1/2} \sin \frac{1}{2}\theta}{|E|^{3/2}} dx \bigg/ \int_0^x \frac{E_\theta^{1/2} \cos \frac{1}{2}\theta}{|E|^{3/2}} dx$$

which is close to  $2\pi \tan \frac{1}{2}\theta$ . The explanation for the observations presumably lies in the amplitude term  $[Y(0)/Y(x)]^{-1/2}$ . A constant difference between the values of  $k$  for the two directions of wave propagation is consistent with an exponential variation of  $Y(x)$ , proportional to  $e^{-\gamma x/\lambda}$ , where  $\gamma$  must be about 0.55 to explain the discrepancy between  $k = 0.85$  peripherally and  $k = 1.40$  centrally. However, the average,  $k \approx 1.13$ , is significantly larger than that predicted from the estimates of  $\tan \theta = \eta\omega/E_{\text{dyn}}$  reported in § 1.1, which give  $2\pi \tan \frac{1}{2}\theta \approx 0.52$ – $0.62$ . Therefore those estimates do not apply to the vessels examined by Hirst & Anliker (1973); the reason for this discrepancy is not readily apparent.

For  $Y = A/\rho c$  to vary with wavelength in the manner predicted above is also inherently unlikely, since we already know, from (1.4), that  $A$  is roughly proportional to  $e^{-\beta x/a}$ , where  $\beta \approx 0.02$ – $0.05$ . Thus

$$c \propto e^{(x/a)(\gamma a/\lambda - \beta)}, \quad (2.58)$$

which increases with peripheral distance only if  $\lambda$  is small enough. This is contrary to observation, which suggests that  $c$  is independent of frequency (i.e. wavelength) and increases approximately linearly with  $x$ :

$$c \approx c_0(1 + nx), \quad n \approx 0.032 \text{ cm}^{-1},$$

(McDonald, 1974). A linear approximation to (2.58) gives  $n \approx \gamma a/\lambda - \beta$ , which is consistent with the quoted numbers only for  $\lambda \approx 10$  cm (frequency  $\approx 50$  Hz), and not for the whole range of frequencies used by Hirst & Anliker (1973). These inconsistencies have no obvious explanation; it would seem that further experiments designed to test (2.55) critically are required.

The above theory shows how the linear wave is modulated by gradual changes in wall properties. A more general theory of a

modulated simple wave has been developed by Seymour (1975) to describe the additional changes brought about by small non-linearities and by weak viscous dissipation. The former tends to steepen the pressure pulse and the latter, like wall viscoelasticity, tends to attenuate it. The development of shocks is predicted if the steepening effects outweigh the dissipative ones. However, like the above elementary theory, Seymour's analysis is restricted in its practical application by the requirement that all amplitude and wave-speed changes should be small over one wavelength of the wave, whereas, in fact, both the taper and the non-linear steepening (§ 2.1) take place over distances short compared with one wavelength of the fundamental cardiac wave. Seymour also makes the unwarranted assumption that the viscous forces in the one-dimensional equation of motion can be represented by a function of the instantaneous average velocity, whereas, in fact, the two are not in phase; this is unimportant in arteries, but only because the fluid viscosity is virtually negligible anyway.

The amplitude gradations predicted by (2.55), in the non-dissipative case where  $Y$  and  $c$  are real, are the same as those predicted from an assumption that the mean energy flux  $\overline{pQ} = Y\overline{p^2}$  down the vessel should be uniform, i.e. no energy is reflected by the gradual taper. Such an assumption is the natural consequence of treating the tapered tube as a sequence of very small isolated discontinuities (Schoenberg, 1968; Lighthill, 1975). To see this and, more importantly, to analyse the effect of arterial junctions, we proceed to analyse the reflection and transmission of waves at junctions.

### 2.3.2 *Isolated wave reflections*

We suppose that a linear wave, with  $p = P_1 f(t - x/c_1)$  is incident from  $x = -\infty$  on a junction at  $x = 0$ . This may take the form of a branching into two or more daughter vessels (fig. 2.6), or may be only a discontinuity in cross-sectional area or elastic properties, which may be either natural (e.g. an arterial stenosis) or artificial (e.g. a cuff round the artery or a junction with a plastic tube). The dimensions of the junction are taken to be small compared with the wavelength of the wave (or any of its Fourier components) so that the vessels can be considered uniform except at  $x = 0$ . Suppose that

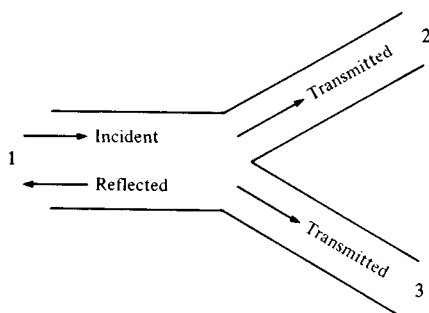


Fig. 2.6. Sketch of an arterial bifurcation. The incident wave is partially reflected in the parent tube 1 and partially transmitted in the daughter tubes 2 and 3.

the parent tube has intrinsic wave speed  $c_1$  and area  $A_1$  so that its characteristic admittance is  $Y_1 = A_1/\rho c_1$ , and let the daughter tubes have wave speed  $c_j$ , area  $A_j$  and admittance  $Y_j = A_j/\rho c_j$ ,  $j = 2, 3 \dots N$ . Note that, in the case of sinusoidal waves, the wave speeds and admittances can be complex. There will be a reflected wave, with associated pressure fluctuation  $p = P_R g(t + x/c_1)$  say, and transmitted waves in each daughter tube, with  $p = P_{Tj} h_j(t - x/c_j)$ . The net flow-rate in the parent tube is

$$Q = Y_1 [P_1 f(t - x/c_1) - P_R g(t + x/c_1)];$$

expressions similar to the first term apply in the daughter tubes.

The conditions to be applied at  $x = 0$  are continuity of flow-rate, to satisfy mass conservation, and of pressure, to satisfy energy (not momentum) conservation. The latter condition requires that viscous losses at the junction are negligible, and that the kinetic energy term proportional to  $\rho Q^2/A^2$  in the expression for the total head is negligible (i.e. that the waves are linear). The conditions can be satisfied only if all waves have the same waveform at  $x = 0$ , so we can take  $g(t) \equiv h_j(t) \equiv f(t)$ . Then continuity of pressure and flow-rate require

$$P_1 + P_R = P_{Tj} \quad (j = 2, 3 \dots)$$

$$Y_1(P_1 - P_R) = \sum_{j=2}^N Y_j P_{Tj},$$

which lead to the following expressions for the amplitudes of the

reflected and transmitted waves:

$$\left. \begin{aligned} P_R/P_I &= \left( Y_1 - \sum_{i=2}^N Y_i \right) / \left( Y_1 + \sum_{i=2}^N Y_i \right), \\ P_{Ti}/P_I &= 2 Y_1 / \left( Y_1 + \sum_{i=2}^N Y_i \right) \quad (i = 2 \dots N) \end{aligned} \right\} \quad (2.59)$$

(as presented by Lighthill (1975), among others).

Restricting attention for now to real values of  $c_i$  and  $Y_i$  (i.e. to non-dissipative waves), we see that if  $\sum_{i=2}^N Y_i < Y_1$ , then the reflected wave has the same sign as the incident wave, the pressures in the two waves are in phase at  $x=0$  and therefore combine additively to form a large-amplitude fluctuation there, and the effect of the junction is similar to that of a closed end (where  $P_R = +P_I$ ). On the other hand, if  $\sum_{i=2}^N Y_i > Y_1$ , there is a phase change at  $x=0$ , the smallest-amplitude pressure fluctuation occurs there, and the junction resembles an open end (where  $P_R = -P_I$ ). If, however,  $\sum_{i=2}^N Y_i = Y_1$ , there is no reflected wave, and the junction is said to be perfectly matched. If the net cross-sectional area increases at a junction, then there should also be an increase in wave speed if the junction is to be perfectly matched. It is interesting to note that the wave speed does indeed increase peripherally, and so does the cross-sectional area. However, this may be misleading since the wave speed also increases with distance down the aorta, while the net cross-sectional area of the circulation does not increase at first (fig. 1.4).

When the reflection is of closed-end type, a sinusoidal incident wave of the form  $p = P_I \cos [\omega(t - x/c_1)]$  will lead to a total pressure fluctuation in the parent tube of

$$p = (P_I - P_R) \cos [\omega(t - x/c_1)] + 2P_R \cos \omega t \cos (\omega x/c_1).$$

Thus the amplitude of the pressure fluctuation will diminish over the first quarter wavelength from the junction (to  $\omega x/c_1 = -\frac{1}{2}\pi$ ) from  $P_I + P_R$  to  $P_I - P_R$ . Now we have seen that in man there tends to be a reduction of area at the iliac bifurcation, suggestive of a closed-end reflection. Therefore, independently of any taper in the aorta, one would expect an increase in amplitude with distance from the heart, as observed. However, similar observations are made in dogs (fig. 1.14), whose aortic trifurcation tends to be quite well

matched, but the amplitude is further increased by occluding the sacral artery in order to create a mis-match (Newman *et al.*, 1973). Thus both taper and the single reflection site at the end of the aorta are implicated in the increase of the pressure pulse along the aorta. Further direct evidence of the isolated reflection site in man can be gathered from fig. 1.17, where a step in the descending part of the velocity waveform can be seen. This step occurs at a time after the start of systole that increases in proportion to the distance *up* the aorta from the iliac bifurcation, reaching a value of about 0.2 s in the innominate artery. The distance from heart to bifurcation and back is about 1.2 m, and the average aortic wave speed is about  $6 \text{ m s}^{-1}$ , so it is consistent to interpret the step as a mark of the wave reflected from the bifurcation. The obvious notch at the end of systole marks the closure of the aortic valve, and is propagated away with the basic pulse, although it is rapidly attenuated because of its high-frequency content. There are so many fluctuations in the pressure and flow-rate waveforms of fig. 1.17 that it is difficult to give any further interpretation in terms of individual waves reflected at isolated sites.

The rate of energy flux associated with a wave is  $pQ = Yp^2$ . Thus the proportion of incident energy reflected is  $P_R^2/P_I^2$ , while the proportion transmitted is  $\sum_{j=2}^N Y_j P_{Tj}^2 / Y_1 P_I^2$ . It can be verified using (2.59) that the sum of these is unity; the former is called the *reflection coefficient*, and the latter the *transmission coefficient*. Note that if a junction is closely, but not perfectly, matched, so that  $P_R/P_I = \epsilon$ , say, then the reflected energy is only  $\epsilon^2$ , which can be negligible. This shows that there can be an observable effect on the incident wave without a diminution of the rate at which energy is transmitted down the system, and explains why the quantity  $Y|p|^2$  remains approximately constant in a very slowly varying vessel (see § 2.3.1).

### 2.3.3 Multiple wave reflections

A full description of the arterial system must include an analysis of the interactions between junctions in a complicated branched network. Consider, for example, a double junction, as illustrated in fig. 2.7, with the single junction already analysed (*B*) attached to the daughter tube of a previous junction (*A*) located at  $x = -l$ . A wave

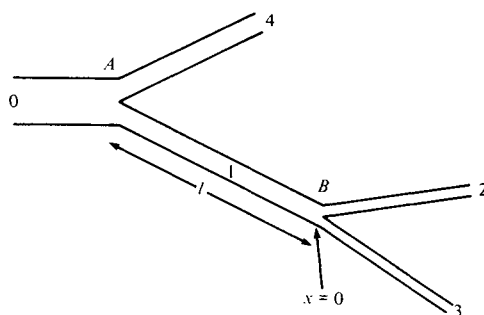


Fig. 2.7. Sketch of a double junction. Wave incident in tube 0 is reflected and transmitted at  $A$ . The transmitted wave in tube 1 is reflected and transmitted at  $B$ , etc.

incident on  $A$  will be partly transmitted there, then partly reflected at  $B$ , re-reflected at  $A$ , and so on (but with ever decreasing amplitude because the reflection is only partial and there is attenuation). The junction at  $A$  can be analysed in exactly the same way as the junction at  $B$  if it is possible to write down a general relation between the pressure and flow-rate in tube  $AB$  at  $x = -l$ , i.e. if there is an *effective* admittance  $Y_{1\text{eff}}$  of the system downstream of  $A$ . Now from the above theory, the ratio of  $Q$  to  $p$  at  $x = -l$  in  $AB$  is

$$Y_{1\text{eff}} = \frac{Q}{p} = \frac{Y_1[f(t+l/c_1) - P_R f(t-l/c_1)]}{f(t+l/c_1) + P_R f(t-l/c_1)}, \quad (2.60)$$

this is very difficult to use because it depends on  $t$ . However, the waves under consideration are periodic and linear, and can therefore be subjected to Fourier analysis. Then, as long as only one frequency is analysed at a time, (2.60) does lead to a constant  $Y_{1\text{eff}}$ : if  $f(t) = e^{i\omega t}$ , then use of (2.59) leads to

$$Y_{1\text{eff}} = Y_1 \left[ \sum_{j=2}^N Y_j + i Y_1 \tan(\omega l/c_1) \right] / \left[ Y_1 + i \sum_{j=2}^N Y_j \tan(\omega l/c_1) \right]. \quad (2.61)$$

Now the junction at  $A$  can be analysed like that at  $B$ , with the *characteristic* admittance of a daughter tube,  $Y_j$ , replaced by its *effective* admittance,  $Y_{j\text{eff}}$ .

Various conclusions can be drawn from (2.61) (Lighthill, 1975). First, if  $l$  is much less than a wavelength,  $\omega l/c_1 \ll 1$ , and  $Y_{1\text{eff}} \approx$

$\sum_{j=2}^N Y_j$  as if the tube  $AB$  were not there. In that case the intermediate tube could be considered as part of the junction. If first order in  $\omega l/c_1$  is retained, we find that

$$Y_{1\text{eff}} \approx \sum_{j=2}^N Y_j + \frac{i\omega l}{c_1} Y_1 \left\{ 1 - \left[ \left( \sum_{j=2}^N Y_j \right) / Y_1 \right]^2 \right\},$$

so that the intermediate tube does not alter the modulus of the effective admittance, but introduces a slight phase lead (or lag) of  $Q$  over  $p$  in the transmitted wave, according as  $Y_1$  is greater or less than  $\sum_{j=2}^N Y_j$ . Note that a similar result is obtained if  $l$  is a whole number of half-wavelengths, so that  $\omega l/c_1$  is an integer multiple of  $\pi$ . There is a resonance, or 'window', effect, because standing waves are set up in  $AB$  (in the absence of attenuation), and the incident wave is 'handed-on' unaltered from  $A$  to  $B$ . In a similar way we can deduce that if  $l$  is an odd number of quarter-wavelengths, so that  $|\tan(\omega l/c_1)|$  is extremely large, then

$$Y_{1\text{eff}} / \sum_{j=2}^N Y_j \approx \left( Y_1 / \sum_{j=2}^N Y_j \right)^2, \quad (2.62)$$

and the relative importance of  $Y_1$  and  $\sum_{j=2}^N Y_j$  is accentuated.

The wavelength of the fundamental mode of the normal pressure pulse in the aorta of man (frequency 1.2 Hz) is about 5 m, roughly eight times the length of the aorta; in a dog (frequency 2 Hz) the wavelength is about 3 m, again about eight times the length of the vessel. Resonance is expected to occur for a mode for which the vessel length is an integer multiple of half the wavelength; in the aorta, therefore, the mode with a frequency of four times the fundamental heart-rate is expected to be closest to resonance. As we shall see, there is normally little evidence of this, presumably because of wave attenuation. The mode with a frequency of twice the heart-rate should be one for which (2.62) is valid, and there is evidence that the modulus of the effective admittance at the entrance to the aorta has a maximum at about twice the fundamental frequency, consistent with (2.62) if  $Y_1 > \sum_{j=2}^N Y_j$  as for a closed-end type of reflection.

The existence of a constant effective admittance for waves of a given frequency, (2.61), means that a complete network can be constructed, starting from pure resistances in vessels of the



microcirculation, and building up junction by junction until a single effective admittance for the whole circulation, appropriate to waves of a given frequency, is arrived at. This is equal to the (complex) ratio between the components of flow-rate and pressure corresponding to the same frequency in the ascending aorta. Its reciprocal is called the *effective* or *input impedance* of the arterial tree; such a quantity is relatively simple to measure for a wide range of naturally occurring frequencies, because all that is needed is Fourier analysis of measured waveforms such as those shown in figs. 1.14 and 1.17. Because of the lack of detailed measurements of lengths and diameters of all arteries in a systemic vascular bed, no complete theoretical predictions have been made. However, Taylor (1966) computed the input admittance for a seven-generation branching network of tubes, whose cross-sectional area decreased and whose wave speed increased peripherally in a physiological way, but in which the distances between branches were arranged at random to simulate the great variety of tube lengths present in the actual circulation. Taylor's results show that the modulus of the input admittance, when plotted against frequency, has a maximum at a frequency for which the length of the 'aorta' is rather less than a quarter-wavelength, and thereafter oscillates about a value equal to the characteristic admittance of the 'aorta'; this value is far above the value at zero frequency, which is the inverse of the overall (peripheral) resistance. The *phase* of the admittance also oscillates about zero, decreasing through zero when the modulus is a maximum (as expected for closed-end reflections). The vigorous oscillations are virtually abolished when wave attenuation is properly accounted for.

McDonald (1974, chapter 13) reports a number of studies in which the effective admittance of different arteries is measured for a range of frequencies. Most measurements are in dogs, some in man. The main conclusions seem to be as follows. The modulus of the admittance in the *ascending* aorta of some dogs has two maxima, one at a frequency of about 2 Hz, and one at about 6 Hz. In other dogs, however, there is a rise in the admittance modulus to a frequency of about 2 Hz, after which there is little change; this observation is roughly consistent with the predictions of Taylor (1966). In the descending *thoracic* aorta, there is never more than

one maximum (at about 2.5 Hz), followed by a marked minimum which itself is absent in more peripheral arteries. In each aortic case the first maximum of the admittance modulus, combined with a zero and falling phase, is interpreted as indicating the presence of a closed-end type of reflection site a quarter-wavelength away. This puts it some distance beyond the end of the aorta in dogs, which suggests (*a*) that the aortic trifurcation is quite well matched (the maximum occurs at a smaller frequency when the sacral artery is blocked (Newman & Bowden, 1973)), and (*b*) that the combined effect of the many peripheral branches is that of a single effective reflection site at about the knee. This is consistent with Taylor's predictions. The subsequent minimum in the admittance modulus presumably reflects the tendency to resonance, so that  $Y_{1\text{eff}}$  is closer to the sum of the admittances of peripheral vessels. The second maximum in the proximal aorta of some dogs is thought to represent another effective site of closed-end reflection in the shorter arteries to the head and forelimbs, which would not have an effect in the descending thoracic aorta (O'Rourke & Taylor, 1967). It is not interpreted as a mode for which the first reflection site is three-quarters of a wavelength away, because (*a*) attenuation would effectively eliminate that, and (*b*) it would be observed in the descending aorta if that were the cause. The absence of the second maximum in  $|Y_{1\text{eff}}|$  in some dogs is thought merely to indicate a less marked difference between the effective impedances of the two arterial systems to the hind- and fore-quarters.

In the ascending aorta of *man* there is just one maximum in  $|Y_{1\text{eff}}|$ , followed by a marked minimum (Mills *et al.*, 1970). The total absence of the second maximum is interpreted as being the result of much greater reflection from the 'hind-quarters' system in man relative to the 'fore-quarters', largely because of the much smaller blood flow to the latter. Furthermore, the reflection site inferred from the first maximum in  $|Y_{1\text{eff}}|$  is much closer to the aortic bifurcation than in dogs, because this is much less well matched in man.

Measurements in the *femoral artery* of a dog also imply a closed-end type of reflection site just below the knee (O'Rourke & Taylor, 1966). Also, the general level of the effective admittance for the first few harmonics of the pulse wave is lower than in the aorta, because

the characteristic admittance is lower on account of the smaller area and lower distensibility of more peripheral arteries.

Mention should finally be made of the *pulmonary circulation*, for which both predictions and measurements of the effective input admittance, as well as of wave speed, have been made. Useful reviews are provided by Milnor (1972) and McDonald (1974). The main results are: (i) A typical value of the wave speed in human pulmonary arteries is about  $1.75 \text{ m s}^{-1}$ , while the corresponding figure in a dog is about  $2.5 \text{ m s}^{-1}$  (see table 1.1). These are roughly consistent with static distensibility measurements. Pulse-wave velocities of  $4\text{--}8 \text{ m s}^{-1}$  have been measured in patients with pulmonary hypertension in which there is pathological thickening and stiffening of vessel walls. (ii) Attenuation studies such as those of Anliker *et al.* (1968*a*) are much more difficult in the short and relatively inaccessible pulmonary arteries, and have not been performed. (iii) The modulus of the input admittance of the pulmonary circulation of a dog has a maximum at a frequency of 3–4 Hz, when the phase becomes zero, which suggests an effective closed-end reflection site in the pulmonary microcirculation. Interpretation in terms of an individual reflection site is even more difficult than in the systemic circulation, because there is no dominant arterial pathway such as that leading through the aorta to the legs. There is a minimum in the admittance modulus at about twice the frequency of the maximum, as one expects if attenuation is not very strong. These results are in qualitative agreement with the theoretical predictions of Wiener *et al.* (1966). The admittance at zero frequency, equal to the reciprocal of the pulmonary vascular resistance, depends strongly on the degree of lung inflation, and reflects a complicated interaction between blood pressure and alveolar air pressure in pulmonary capillaries, which is beyond the scope of this monograph.

#### 2.4 Non-linear models of a complete arterial pathway

We have seen that linear theories can give a reasonable description of the propagation, reflection and attenuation of the pulse wave in a branched network of arteries, as long as the area and distensibility of the arteries vary only very gradually with distance between the

junctions. However, this condition is not normally satisfied. Furthermore, there are a number of phenomena, especially abnormal ones, that can be accounted for only by non-linearities (§ 2.1). (This is also true of the development of the mean flow, which according to linear theory is Poiseuille flow everywhere; this aspect is further examined in chapter 3.) In this section, therefore, a method that has been used to analyse non-linear phenomena in an arterial pathway that is not necessarily very slowly varying is outlined; certain drawbacks in the method, at least as practised hitherto, are discussed.

A single arterial pathway, from the heart to a capillary bed, is modelled as a single tube whose cross-sectional area and distensibility vary with distance along it. It is assumed that a one-dimensional theory such as that of § 2.1 can be applied; this means that  $u(x, t)$  is the average velocity across a cross-section and that  $p(x, t)$  is the average pressure. It is not necessary that a length-scale of longitudinal variation in tube properties be large compared with a wavelength, as in § 2.3, but it is desirable that the length-scale be significantly greater than the tube diameter, both in order that  $p$  should approximately represent the pressure measured in the centre of the vessel as well as the average, and so that the numerical methods to be employed do not need absurdly small step lengths. The branching of the arterial tree is modelled by letting the tube have 'porous' walls, with a volume outflow  $\psi$  per unit length. In reality  $\psi$  will be a function of position with sharp discontinuities, and users of the porous-tube model have invariably smoothed it out considerably. However, wave reflections can still be analysed nearly as accurately as in § 2.3, because there it was assumed that the junction, which really occupies a finite length of tube, was concentrated at a point. In this model it is spread out again, in such a way as to leave the reflection coefficient of the junction unaltered (in principle, at least; I know of no-one who has actually verified this aspect of their outflow model). The idea of modelling an artery as a tapered, porous tube seems to have originated with Streeter, Keitzer & Bohr (1963), and was developed further by Skalak & Stathis (1966). The most thorough investigation of such a model is the simulation of the canine systemic circulation by Anliker *et al.* (1971), and it is to their work that I shall refer most often.

The equations relating velocity  $u(x, t)$ , excess pressure  $p(x, t)$  and area  $A(x, t)$  are similar to, but more general than, (2.1)–(2.3), as follows.

Mass conservation:

$$A_t + (uA)_x + \psi = 0. \quad (2.63)$$

Momentum equation:

$$u_t + uu_x + (1/\rho)p_x = f. \quad (2.64)$$

Wall properties:

$$A = A(\tilde{p}, \tilde{p}_t, x), \quad (2.65)$$

where

$$\tilde{p} = p - P_0(x, t). \quad (2.66)$$

In (2.65) and (2.66)  $\tilde{p}$  is the transmural pressure, which may not be equal to the excess pressure  $p$  if either there is a variable external pressure or there is a significant variation of hydrostatic pressure within the tube. These effects are represented by the function  $P_0(x, t)$ ; in the latter case  $P_0 \equiv -\rho g'x$ , where  $g'$  is the component of the gravitational acceleration in the  $x$ -direction. The distensibility, viscoelasticity and taper of the vessel are represented by the dependence of  $A$  on  $\tilde{p}$ ,  $\tilde{p}_t$  and  $x$ , respectively. Equation (2.64) is derived from the integral momentum equation (because  $u$  is really the average cross-sectional velocity,  $\bar{u}$ ) on the assumptions (a) that the difference between  $\bar{u}^2$  and  $(1/A) \int u^2 dA$  is negligible, which is reasonable when the velocity profile in the core of the tube is flat with thin boundary layers outside it, as for oscillatory flow at large  $\alpha$  (§ 2.2); and (b) that the  $x$ -momentum convected from the tube by the outflow is equal to  $\rho u \psi$  per unit length (Schaaf & Abbrecht, 1972). The quantity  $f$  in (2.64) is the viscous retarding force, approximately equal to  $-\tau S/\rho A$  where  $\tau$  is the average shear stress at the wall (assumed approximately parallel to the  $x$ -direction) and  $S$  is the tube perimeter.

The equations can be reduced to characteristic form as in § 2.1. Define the intrinsic wave speed,  $c$ , by

$$c^{-2} = (\rho/A) \partial A / \partial \tilde{p}, \quad (2.67)$$

and then add  $\pm c/A$  times (2.63) to (2.64) to obtain

$$u_t + (u \pm c)u_x \pm (1/\rho c)[\tilde{p}_t + (u \pm c)\tilde{p}_x] \\ = f - (1/\rho)P_{0x} \mp (c/A)(\psi + uA_x) \mp (c\tilde{A}_{\tilde{p}l}/A)(\tilde{p}_{tt} + u\tilde{p}_{tx}). \quad (2.68)$$

Thus on the characteristic curves  $C_{\pm}$ , defined by  $dx/dt = u \pm c$ , the quantities  $(d/dt)(u \pm \int d\tilde{p}/\rho c)$  are given by the right-hand side of (2.68). If the right-hand side is known in terms of  $u$ ,  $p$ ,  $x$ ,  $t$  at all values of  $x$  and  $t$ , the equations can be solved by a straightforward numerical integration forward in time along the characteristics, and this is what almost all workers hitherto have done. Assuming that the functions  $P_0(x, t)$  and  $A(\tilde{p}, \tilde{p}_n, x)$  are given, the terms to be considered further are  $\psi$ ,  $f$ , and the last term on the right-hand side of (2.68), which represents the viscoelasticity of the wall.

### Outflow

The outflow function  $\psi$  can clearly not be given as a function of  $x$  and  $t$ , because the outflow through side-tubes depends on the pressure and/or flow-rate in the parent (§ 2.3). The best choice for  $\psi$  would be one that incorporated measurements or predictions of the input admittance of each side-branch. However, the admittance is normally frequency-dependent, so implementation of this choice would require time Fourier analysis of the pressure waveform at each value of  $x$ ; but in the conventional technique of integrating along characteristics,  $p$  is known only for times past. This specification of  $\psi$  would therefore require an iterative solution of (2.68): a first guess at the solution would yield an estimate for  $\psi$ , which would be used in the conventional integration of the equations; the result of that integration would be used to supply the next estimate of  $\psi$ , and so on. This approach would be relatively expensive in computer time (although it would converge rapidly if the effect of  $\psi$  were small), and I know of no-one who has followed it. An alternative approach would be to abandon the characteristic equations, and solve the complete problem by a finite-difference method; this has been done by Raines, Jaffrin & Shapiro (1974) for the arteries in the leg. These authors also proposed a useful model for outflow, in which each of the most important side-branches was simulated by means of a linear lumped-parameter system with two

given resistances and a compliance in series. These branches occurred at points and were not smoothed out. The results of this analysis suggested rather surprisingly (but in agreement with experiment) that occlusion of the side-branches has little effect on the propagating pressure pulse. This is not true of the model of Anliker *et al.* (1971), described further below.

What most authors using the characteristic method have done is to specify  $\psi$  in terms either of  $p$  or of  $u$  in the parent tube. Anliker *et al.* (1971), following Streeter *et al.* (1963), assumed a constant peripheral resistance (and no compliance) in each branch, and proposed that

$$\psi = f_1(x)(p - p_c), \quad (2.69)$$

where  $p_c$  is a given end-capillary pressure and  $f_1(x)$  is a function chosen to simulate approximately the measured distribution of blood flow to different regions of the body. Anliker *et al.* took

$$\begin{aligned} f_1(x) &= \gamma[1.1 + \cos(5\pi x/2x^*)] \quad \text{for } x \leq x^* \\ &= \gamma \times 1.1 \times e^{-0.08(x-x^*)} \quad \text{for } x \geq x^*, \end{aligned}$$

where  $x^* \approx 70$  cm (for a 30-kg dog) and  $1/\gamma$  is a measure of outflow resistance, which can be varied to simulate different experimental conditions.

Skalak & Stathis (1966) analysed a symmetric dichotomously branching network, in which all branches were geometrically similar (quite a good model of the *pulmonary* arterial tree), by recognising that every branch in a given generation of branching would receive the same flow-rate, equal to half the flow-rate in a tube of the preceding generation. They therefore took

$$\psi = \alpha m Au / (1 - mx), \quad (2.70)$$

which is equal to  $d(Au)/dx$  when  $Au = q_1(1 - mx)^\alpha$ . Here  $q_1$  is the steady flow-rate in the parent tube of a similar *rigid* network,  $\alpha = \frac{1}{2} \log 2 / \log \beta$ , where  $\beta$  is the ratio of the cross-sectional area of a daughter tube to that of the parent at a junction, and  $m$  is the constant in the linear relation between the square root of area and distance down the system:  $A^{1/2} \propto 1 - mx$ . From the point of view of integrating (2.68), both (2.70) and (2.69) are equally simple.

*Viscous friction*

The analysis of § 2.2 suggests that the quantity  $f$  would be accurately given by Womersley's (1955) analysis of oscillatory flow in a rigid tube. Thus if the pressure gradient at any  $x$  were Fourier analysed in time to give

$$\frac{dp}{dx} = \sum_{n=0}^{\infty} G_n(x) e^{in\omega t},$$

where  $G_n(x)$  is complex, the frictional drag  $f$ , equal to  $-2\tau/ap$  for a circular tube (which we assume) would be

$$f = \frac{1}{\rho} \sum_{n=1}^{\infty} G_n(x) F(\alpha_n) e^{in\omega t} + \frac{G_0}{\rho} \quad (2.71)$$

from (2.49), where  $G_0$  is the mean pressure gradient ( $<0$ ) and  $\alpha_n^2 = n\omega a^2/\nu$ ;  $F(\alpha)$  is given by (2.37). For large  $\alpha$ , which is appropriate here for at least the largest arteries in the pathway studied,  $F \sim 2/\alpha^{1/2}$ . However, the use of (2.71), like that of a proper outflow function, requires Fourier analysis of the pressure gradient, and therefore an iterative numerical method is needed. Instead, most authors have assumed that  $f$  is in phase with  $u$  and depends on it alone, and many, including Anliker *et al.* (1971) and Schaaf & Abbrecht (1972) have taken it to be quasi-steady, either for laminar flow ( $f = -8\pi\nu u/A$ ) or for turbulent flow ( $f = -0.14\nu^{1/4}|u|^{3/4}u/A^{5/8}$ ). Olsen & Shapiro (1967) used the quasi-steady relation for turbulent flow when the Reynolds number exceeded 3000, but used the real part of the complex relation between  $\tau$  and  $Q(=uA)$ , obtained from (2.48) and (2.49), for laminar flow; however, they were dealing with only small departures from a single sinusoidal mode. Since the effect of viscosity on wave propagation is small when  $\alpha$  is large (§ 2.3; see also Olsen & Shapiro, 1967), these approximations are unlikely to cause great inaccuracy in predictions made for large arteries. However, for pathways containing significant portions of small arteries, where  $\alpha$  may be relatively small (less than about 4), the effect of friction will be greater and these models inaccurate. This is particularly true of the model of the coronary circulation developed by Rumberger & Nerem (1977).



*Viscoelasticity*

This is known to be the principal factor causing wave attenuation in arteries, and is likely to be important in all arterial pathways except those so short that attenuation is unimportant (the aorta alone, for example). However, the last term in (2.68) is very complicated, and I know of no integrations in which it has been taken into account. Indeed, it is not possible to take it into account and still to be able to march forward in time, integrating once along the characteristics, because in even the simplest, linear, model of wall viscoelasticity, in which

$$A = A_1(\tilde{p}, x) - \tilde{p}_t B(\tilde{p}, x)$$

(cf. (2.19) and (2.20)), the term  $\tilde{p}_{tt} + u\tilde{p}_{tx}$  is still present. Thus to take wall viscoelasticity into account, it is *necessary* to solve the problem either iteratively along the characteristics, which is suitable if this term is relatively small, or by a finite-difference method. This, together with a more adequate treatment of outflow, is the most important next step in the non-linear numerical modelling of wave propagation in arteries.

*Elastic properties*

Anliker *et al.* (1971) defined the elastic properties of their aortic pathway by specifying  $c$  as an empirically determined function of  $\tilde{p}$  and  $x$ :

$$c(\tilde{p}, x) = (c_0 + c_1\tilde{p})(1 + nx), \quad (2.72)$$

where  $c_0 = 97 \text{ cm s}^{-1}$ ,  $c_1 = 15.3 \text{ cm s}^{-1} \text{ per kN m}^{-2}$  and  $n = 0.02 \text{ cm}^{-1}$ . They also specified the area as a function of  $x$  at a particular value of  $\tilde{p}$  ( $p_0 = 13.3 \text{ kN m}^{-2}$ ):

$$\begin{aligned} A(p_0, x) &= 4.63 e^{-0.045x} & \text{for } x \leq 54 \text{ cm} \\ &= 0.41 e^{-0.089(x-54)} & \text{for } x \geq 54 \text{ cm}. \end{aligned}$$

Thus they obtained

$$A(\tilde{p}, x) = A(p_0, x) \exp [(\tilde{p} - p_0)/\rho c(\tilde{p}, x)c(p_0, x)].$$

They ignored  $P_0(x, t)$  and viscoelasticity in their model, and could integrate directly.

Note that a particularly simple integration of (2.68) is possible if the simple elastic properties given by (2.11) are chosen. Then the

left-hand side is

$$(d/dt)(u \pm c) \equiv \frac{1}{2}(d/dx)[(u \pm c)^2]$$

on the characteristics  $C_{\pm}$ . Riemann invariants can be found if the right-hand side can also be expressed as  $d/dx$  of something on  $C_{\pm}$ , or as  $u \pm c$  times  $d/dx$  of something. No such case naturally arises, except when attenuation, outflow and taper are negligible, and the effect of an external pressure  $P_0(x)$ , which is constant in time but relatively rapidly varying in  $x$ , is to be analysed. Then  $\frac{1}{2}(u \pm c)^2 + (1/\rho)P_0(x)$  is constant on  $C_{\pm}$ .

### *Boundary conditions*

The conditions at  $x = 0$  are those at the exit of the heart, in the aorta or in the pulmonary artery according to which circulatory bed is being modelled. In principle, one may specify (by measurement) either  $p(0, t)$  or  $u(0, t)$  (or a combination of the two involving the measured input admittance of the system), but Anliker *et al.* (1971) found that much more satisfactory results were obtained by specifying  $u(0, t)$ , because the numerical procedure was less sensitive to small variations in this quantity. Downstream conditions, at  $x = L$  ( $= 150$  cm) can most conveniently be expressed in terms of a constant peripheral resistance  $R_L$ , so that

$$A[p(L, t), L]u(L, t) = [p(L, t) - p_c]/R_L,$$

where  $p_c$  is the end-capillary pressure (as in (2.69)).  $R_L$  was given a value that yielded the correct mean pressure at  $x = 0$ .

Various initial conditions at  $t = 0$  may be chosen. The standard case in Anliker *et al.*'s computation was one in which conditions at the start of systole were close to those at the end of diastole (periodicity condition), requiring more than one integration of (2.68). Another possibility is to suppose that, at  $t = 0$ , the blood is at rest with a given pressure.

### *Results*

The results of computer models such as this always show a broad qualitative agreement with experiment, even without an adequate treatment of wall viscoelasticity, fluid viscosity, or outflow. The standard results of Anliker *et al.* (1971) clearly show peaking and

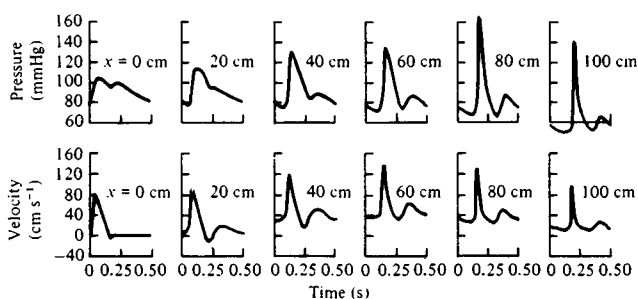


Fig. 2.8. Predicted pressure and velocity waveforms at six different locations along the artery;  $x = 0$  is the aortic valve. (After Anliker *et al.*, 1971.)

steepening of the pressure pulse, the development of a second peak in the pressure pulse, and the development of considerable reverse flow in the abdominal aorta (fig. 2.8). However, the usual fall-off in peak velocity with distance and the persistence of backflow into more peripheral arteries are not seen. These features of the results reveal the shortcomings of the model; in my view, its chief defect lies in the excessively smooth and inaccurate form chosen for the outflow function  $f_1(x)$  in (2.69). The only direct evidence for this, however, is that varying the outflow constant  $\gamma$  over a reasonable physiological range had a more marked effect on the results than varying the friction factor  $f$ . No different shape for  $f_1(x)$  was used; neither was any viscoelasticity taken into account. We may note further that the cumulative effect of non-linearities was not negligible (fig. 2.9), as found also by Schaaf & Abbrecht (1972) and by Ling *et al.* (1973) (the latter authors used a different method; see chapter 3).

Perhaps the greatest value of models such as this is the simulation of different clinical conditions, so that either observed abnormalities may be explained or possible abnormalities can be predicted. Anliker *et al.* (1971) considered a number of examples. One of particular interest is the modelling of aortic valve incompetence by the imposition of a very-large-amplitude velocity waveform at  $x = 0$ . The model predicts that very sharp pressure and velocity peaks are formed for  $x$  lying between 50 and 100 cm, the thickness of the wavefront being as little as 6 cm. The authors interpret these results (*a*) as explaining the arterial 'pistol-shot' pulse observed in

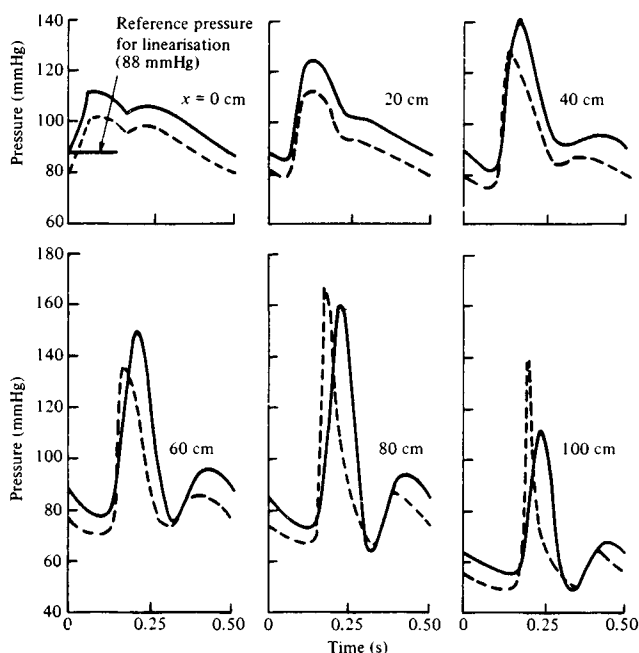


Fig. 2.9. Comparison of pressure waveforms predicted from non-linear (broken curves) and linearised (continuous curves) theory. (After Anliker *et al.*, 1971.)

the limbs of patients with incompetent valves and (b) as indicating the presence of shocks. While it is probable that shocks do occur when such sharp pressure pulses are formed, they cannot arise out of a numerical integration along characteristics unless the integration breaks down and two characteristics cross. In that case jump conditions have to be applied across the shock, involving extra dissipation (§ 2.1). Anliker *et al.* did not refer to such numerical breakdown, and it is possible that shocks did not actually appear in their model. Any errors would no doubt be largely due to the assumption that outflow was linearly related to local pressure, by a peripheral resistance, and this would be particularly inaccurate for such sharp pressure peaks since shocks would be formed in side-branch arteries also. The absence of viscoelasticity would also make the model markedly inaccurate when such steep waves are predicted. These authors also noted, but did not model, a 'venous pistol

shot', heard over the jugular and femoral veins when the tricuspid valve (between right atrium and ventricle) is incompetent; this phenomenon is described by Hultgren (1962). Anliker *et al.* did not report the input admittance of the arterial system as predicted by their model; Schaaf & Abbrecht (1972) did compute it, and that of the femoral artery, although their model had a less-well-founded description of arterial elasticity. They were able to reproduce some of the measured features described above, such as a more marked maximum of the admittance modulus in the femoral bed than in the aortic bed, but qualitative similarity with observation is to be expected. Future models must either show how to incorporate real features hitherto absent (such as viscoelasticity) or be able to describe quantitatively phenomena that have not previously been accurately modelled.

An arterial bed of particular clinical importance is the coronary circulation. Rumberger & Nerem (1977) have applied a model very similar to that of Anliker *et al.* (1971) to a pathway in the horse, starting at the left coronary ostium and incorporating the left common coronary artery and the left anterior descending artery. There are two important differences between this model and one starting in the aorta. First, the vessels are smaller, so fluid viscosity will have a greater influence (and should therefore be modelled more accurately, but this was not done). Secondly, the pathway plunges into the heart muscle at about 25 cm from the entrance, and this muscle exerts a strong, but variable, external pressure  $P_0(x, t)$  (see (2.66)). The authors appreciated this, and used left ventricular pressure (times a known function of  $x$ ) as the external pressure, which is a reasonable first approximation. However, they still used an equation similar to (2.72) to describe arterial elasticity, which ignores the greater distensibility expected in blood vessels when the transmural pressure is low (cf. fig. 1.10). Much less information on wave propagation is available in coronary arteries than in the aorta, and Rumberger & Nerem derived the elastic constants for their model from a few experiments of their own. They also ignored viscoelasticity, like everyone else. Nevertheless, despite the shortcomings of the model, they were able to reproduce pressure and velocity waveforms that exhibit the principal observed features: (i) a much greater flow-rate in diastole when the squeezing of the

peripheral part of the pathway is lifted, and (ii) high-frequency ( $\sim 10$  Hz) oscillations in pressure and velocity (fig. 1.19). Since the oscillations occur in the model, they must represent a resonance phenomenon involving a Fourier mode for which the length of the pathway to the major reflection site (perhaps where the artery enters the muscle at  $x = 25$  cm) is a half-wavelength. A frequency of 10 Hz and a wavelength of 50 cm means a wavespeed of  $5 \text{ m s}^{-1}$ , which is reasonably consistent with the wave-speed values put into the model by Rumberger & Nerem.